Miner Petrol (2014) 108:419–438
DOI 10.1007/s00710-013-0310-6

ORIGINAL PAPER

Platinum-group element geochemistry of the Zhuqing Fe-Ti-V oxide ore-bearing mafic intrusions in western Yangtze Block, SW China: control of platinum-group elements by magnetite

Hong-Peng Fan · Wei-Guang Zhu · Hong Zhong · Zhong-Jie Bai · De-Feng He · Xian-Tao Ye · Cai-Jie Chen · Chong-Yong Cao

Received: 10 December 2012 / Accepted: 22 August 2013 / Published online: 6 September 2013

Abstract Platinum-group element (PGE) geochemistry combined with elemental geochemistry and magnetite compositions are reported for the Mesoproterozoic Zhuqing Fe–Ti–V oxide ore-bearing mafic intrusions in the western Yangtze Block, SW China. All the Zhuqing gabbros display extremely low concentrations of chalcophile elements and PGEs. The oxide-rich gabbros contain relatively higher contents of Cr, Ni, Ir, Ru, Rh, and lower contents of Pt and Pd than the oxide-poor gabbros. The abundances of whole-rock concentrations of Ni, Ir, Ru, and Rh correlate well with V contents in the Zhuqing gabbros, implying that the distributions of these elements are controlled by magnetite. The fractionation between Ir–Ru–Rh and Pt–Pd in the Zhuqing gabbros is mainly attributed to fractional crystallization of chromite and magnetite, whereas Ru anomalies are mainly due to variable degrees of compatibility of PGE in magnetite. The order of relative incompatibility of PGEs is calculated to be Pd<Pt<Rh<Ir<Ru. The very low PGE contents and Cu/Zr ratios and high Cu/Pd ratios suggest initially S-saturated magma parents that were highly depleted in PGE, which mainly formed due to low degrees of partial melting leaving sulfides concentrating PGEs behind in the mantle. Moreover, the low MgO, Ni, Ir and Ru contents and high Cu/Ni and Pd/Ir ratios for the gabbros suggest a highly evolved parental magma. Fe–Ti oxides fractionally crystallized from the highly evolved magma and subsequently settled in the lower sections of the magma chamber, where they concentrated and formed Fe–Ti–V oxide ore layers at the base of the lower and upper cycles. Multiple episodes of magma replenishment in the magma chamber may have been involved in the formation of the Zhuqing intrusions.

Editorial handling: J. G. Raith

H.-P. Fan · W.-G. Zhu (✉) · H. Zhong · Z.-J. Bai · D.-F. He · X.-T. Ye
State Key Laboratory of Ore Deposit Geochemistry, Institute of Geochemistry, Chinese Academy of Sciences, 46 Guanshui Road, Guiyang 550002, China
e-mail: zhuweiguang@vip.gyig.ac.cn

H.-P. Fan · X.-T. Ye
University of Chinese Academy of Sciences, Beijing 100049, China

C.-J. Chen · C.-Y. Cao
Geological Team 601, Sichuan Bureau of Metallurgical Geology and Mineral Exploration, Panzhihua 617027, China

Introduction

Magnetite-bearing layers formed from highly fractionated magmas in the upper parts of layered intrusions worldwide are often depleted in platinum-group elements (PGEs: Os, Ir, Ru, Rh, Pt, and Pd) due to the likelihood that PGE have already been removed from the parental magma by sulfide liquid separation or previous crystallization of platinum-group minerals (PGMs) (e.g., Sá et al. 2005). However, PGE enrichments in magnetite-bearing cumulates are present in some intrusions, such as the Xinjie intrusion in SW China (Zhong et al. 2011), the Rio Jacaré intrusion in Brazil (Sá et al. 2005), the Bushveld Complex (Harney et al. 1990; Barnes et al. 2004) and the Stella Intrusion in South Africa (Maier et al. 2003). There is also some experimental evidence showing that magnetite concentrates Ru at high oxygen fugacities (fO_2) (Capobianco et al. 1994; Righter 2001; Brenan et al. 2012). Magnetite-bearing rocks from the lower part of the Upper Zone of the Bushveld Complex have much lower Pd/Ir ratios (Harney et al. 1990) than those of the marginal rocks (Davies and Tredoux 1985; Barnes and Maier 2002), suggesting that magnetite concentrated Ir relative to Pd. Furthermore, Barnes et al. (2004) supposed that magnetite concentrates Ir and Rh in preference to Pt, Pd, and Au in the Main Magnetite Layer in the Bushveld Complex. Thus, magnetite seems to preferentially fractionate Ir, Ru, and Rh compared to Pt and Pd. However, it is still difficult to determine the controlling effects of the Fe–Ti oxides on PGEs

in the presence of sulfide because sulfides and sulfide liquid have much higher partition coefficients for PGEs than magnetite (Stone et al. 1990; Bezmen et al. 1994; Peach et al. 1994; Fleet et al. 1996; Crocket et al. 1997; Barnes et al. 2004; Fonseca et al. 2009). It has been widely accepted that the distribution of PGEs in mafic and ultramafic rocks is most commonly controlled by sulfides, chromite, olivine and PGMs (e.g., Barnes et al. 1985). Therefore, further work should be conducted to investigate whether PGEs are controlled by Fe–Ti oxides in some mafic and ultramafic rocks.

PGEs in combination with Ni and Cu contents could provide valuable information on the petrogenesis of mafic–ultramafic rocks (e.g., Lightfoot and Keays 2005; Maier 2005). The Zhuqing gabbroic intrusions in the western Yangtze Block that host Fe–Ti–V oxide ore deposits were likely the products of a mantle plume that contributed to the break-up of the Paleo- to Mesoproterozoic supercontinent Columbia/Nuna. Moreover, it has been suggested that the intrusions fractionally crystallized from a parental magma generated by low degrees of partial melting of a slightly enriched asthenospheric mantle source (Fan et al. 2013). The Zhuqing intrusions, which host Fe–Ti oxides mineralization but are poor in PGE–sulfide mineralization, offer a good chance for investigating to which extent PGEs are controlled by magnetite. In this paper, we present PGE data combined with major and trace element abundances, as well as magnetite compositions determined by electron microprobe for the Zhuqing Fe–Ti–V oxide ore–bearing mafic intrusions with the aims to (1) discuss PGE fractionation and the controls of PGEs in the Fe–Ti–V oxide ore-bearing rocks and (2) shed new light on the petrogenesis and mineralization in the Zhuqing intrusions.

Geological background and petrography

The South China Block consists of two major Precambrian blocks: the Yangtze Block to the northwest and the Cathaysia Block to the southeast (present coordinates), with the late-Mesoproterozoic to earliest Neoproterozoic Sibao Orogen situated between them (Fig. 1a). There are sparse ~2900 Ma rocks in the northern part of the Yangtze Block (Gao et al. 2001). However, ancient lower crustal xenoliths (Zheng et al. 2006) and abundant Archean to Paleoproterozoic detrital zircon in the Meso- to Neoproterozoic sedimentary sequences (Sun et al. 2009; Zhao et al. 2010; Wang et al. 2013) indicate the existence of widespread Archean to Paleoproterozoic basement rocks. Widely distributed Proterozoic strata are typically thought to be folded basement of the Yangtze Block and these strata are uncomfortably overlain by an unmetamorphosed Sinian to Cenozoic cover sequence (Yan et al. 2003).

The Kangdian area (Fig. 1b) is located near the western margin of the Yangtze Block, South China (Fig. 1a). The oldest supracrustal rocks in this area are the late Paleo- to Mesoproterozoic meta-volcanic and sedimentary rocks of the Dahongshan Group (Greentree and Li 2008), the Dongchuan Group (Zhao et al. 2010), the Hekou Group (Wu et al. 1990; He 2009; Zhao and Zhou 2011), the Huili Group (Yin et al. 2011), and the Kunyang Group (Yin et al. 2011), occurring along the Luzhijiang fault and a series of related NNE-trending faults (Figs. 1b and 2a). They consist of meta-sedimentary rocks interbedded with felsic and mafic meta-volcanic rocks, for example, the Dahongshan, Hekou, Dongchuan, and Huili groups contain mafic intrusions and meta-volcanic layers with zircon U–Pb ages of 1.5–1.7 Ga (Chang et al. 1997; Greentree and Li 2008; He 2009; Zhao et al. 2010; Zhao and Zhou 2011; Fan et al. 2013), and the Huili and Upper Kunyang groups have meta-volcanic layers with zircon U–Pb ages of ~1.0 Ga (Chang et al. 1997; Mou et al. 2003; Greentree et al. 2006; Geng et al. 2007; Zhang et al. 2007). These rocks are overlain by a thick sequence (maximum >9 km) of Neoproterozoic (850–540 Ma) to Permian strata composed of clastic, carbonate and volcanic rocks.

A number of mafic intrusions including the Zhuqing intrusions intruded dolostones and slates of the Mesoproterozoic Heishan Formation of the Huili Group in the Tong'an area, SW China (Fig. 1b). These intrusions, dominantly composed of alkaline gabbroic rocks, are distributed as dykes or irregular small intrusions (Fig. 2a). The Zhuqing intrusions are bounded by a series of faults in the northeast of the Tong'an area (Fig. 2b). The mafic intrusions are up to 4 km long and commonly 90–370 m wide, striking NW 303°–349° and dipping ~45°–65° to the southwest. Intrusions I and II host Fe–Ti–V oxide ore deposits in their lower zones. Most of the intrusions consist of medium- to coarse-grained gabbros, and the mineral grains are typically larger in the lower zone (Fig. 3a) than those in the upper zone of the intrusions (Fig. 3b). These gabbros can be divided into oxide-rich and oxide-poor gabbros based on whole-rock Fe_2O_3 contents. The oxide-rich gabbros (Fe_2O_3 > 29 wt.%) consist of >20 vol.% Fe–Ti oxides (magnetite and ilmenite), approximately 40 vol.% plagioclase, 30 vol.% clinopyroxene, and minor amounts of hornblende, biotite and sulfide minerals,whereas the oxide-poor gabbros contain 40–60 vol.% plagioclase, 30–40 vol.% clinopyroxene, 5–10 vol.% Fe–Ti oxides and minor amounts of sulfide minerals, apatite, hornblende and biotite. The magnetites in the Zhuqing gabbros have ilmenite exsolutions with different shapes such as trellis-shaped or of a more coarse-grained type (Figs. 3a, f). The Zhuqing intrusions are divided into three cycles from the base to the top: a marginal cycle (zone 1), a lower cycle (zones 2 and 3), and an upper cycle (zones 4 and 5) (Fig. 4). The marginal cycle, located at the base of the intrusions, is mainly composed of coarse plagioclase, clinopyroxene, Fe–Ti oxides, and minor amounts of apatite. The lower cycle is composed of a Fe–Ti oxide cumulate layer interbedded with thin gabbroic layers (zone 2) and an overlying medium- to coarse-grained gabbroic layer

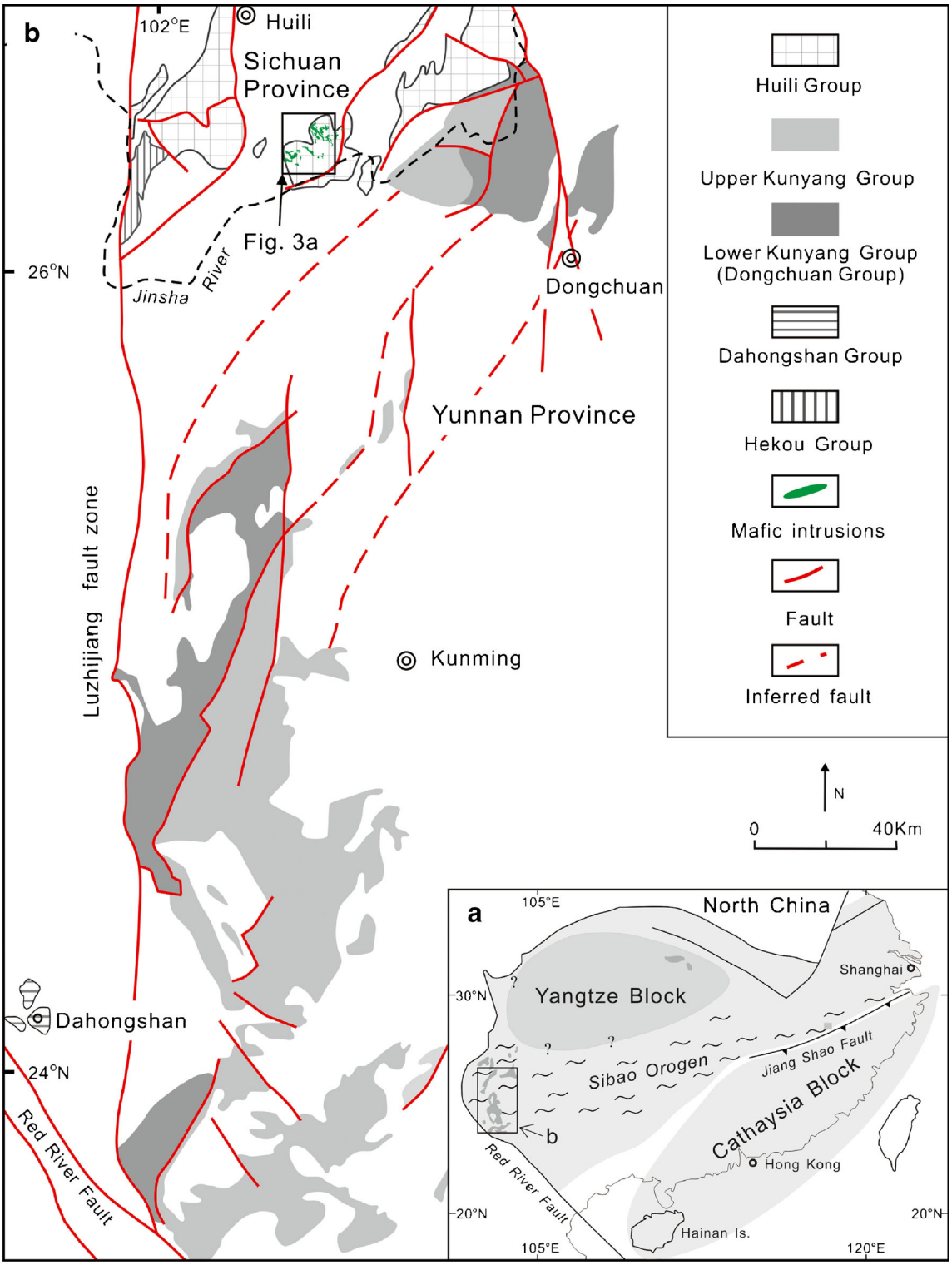

Fig. 1 **a** Simplified tectonic map showing the study area in relation to major tectonic units in South China (Li et al. 2007); **b** Geological map of Precambrian supracrustal rocks and Neoproterozoic intrusions in the Kangdian region, SW China (modified from Wu et al. 1990)

(zone 3). The upper cycle is similar to the lower cycle except that mineral grains are smaller in the upper cycle and apatite and sulfide minerals are more common in zone 5 of the upper cycle (Fig. 4).

Sampling and analytical methods

In this study, twenty-four samples were collected from the drill cores ZK2801 and ZK3602. The drill core locations are shown

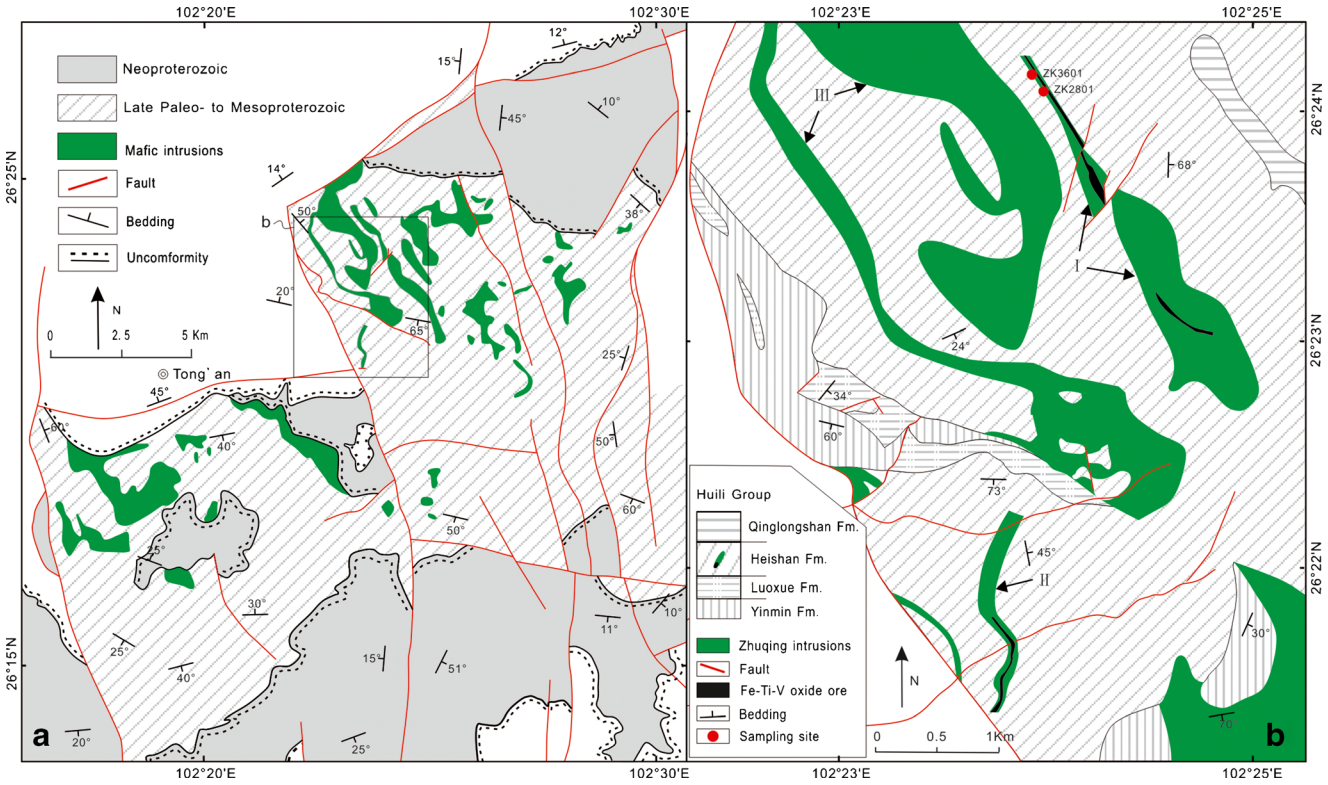

Fig. 2 **a** Simplified geological map of the Mesoproterozoic to earliest Neoproterozoic rocks in the Tong'an region, SW China; **b** Geological map of the Zhuqing intrusions and sampling locations

in Fig. 2b. Drill core samples were crushed to 200-mesh using an agate mill for whole-rock geochemical analyses.

Whole-rock major element compositions were determined by X-ray fluorescence spectrometer (XRF) at the State Key Laboratory of Isotope Geochronology and Geochemistry, Guangzhou Institute of Geochemistry, Chinese Academy of Sciences (CAS) and the Mineral Division of ALS Laboratory Group, Guangzhou, using fused lithum-tetraborate glass pellets. The analytical precision is better than 5%.

Whole rock trace element compositions were analyzed using a Perkin-Elmer Sciex ELAN DRC-e ICP-MS at the State Key Laboratory of Ore Deposit Geochemistry (SKLODG), Institute of Geochemistry, CAS (IGCAS). The powdered samples (50 mg) were dissolved in high-pressure Teflon bombs using $HF+HNO_3$ mixture for 48 h at ~190 °C (Qi et al. 2000). Rh was used as an internal standard to monitor signal drift during counting. The international standards GBPG-1, OU-6, and the Chinese National standards GSR-1 and GSR-3 were used for analytical quality control. The analytical precision is generally better than 5% for trace elements. Sulfur contents were determined by a C-S analyzer at the SKLODG, IGCAS (Appendix 1).

Platinum-group elements were determined by isotope dilution (ID)-ICP-MS (Perkin-Elmer Sciex ELAN DRC-e) using an improved digestion technique at the SKLODG, IGCAS (Qi et al. 2011). The mono-isotopic element Rh was measured by external calibration using a ^{194}Pt spike as internal standard (Qi et al. 2004). Eight grams of rock powder were first digested by HF in a custom made 120 ml PTFE beaker on a hot plate to remove silicates, after that, the dried residue with appropriate amount of enriched isotope spike solution containing ^{193}Ir, ^{101}Ru, ^{194}Pt, and ^{105}Pd was digested with $HF + HNO_3$ at 190 °C for about 48 h after the beaker is sealed in a stainless steel pressure bomb (Qi et al. 2011). The total procedural blanks were lower than 0.002 ppb for Ir and Rh, 0.015 ppb for Ru, 0.002 ppb for Pt, and 0.040 ppb for Pd. The accuracies were estimated to be better than 10% for all PGE (Appendix 2).

The compositions of magnetite were determined by a JXA-8100 electron microprobe wavelength-dispersive spectrometry at the State Key Laboratory of Lithospheric Evolution, Institute of Geology and Geophysics, CAS. The beam current was 20 nA with acceleration voltage of 15 kV and beam size of 1 μm. Both natural and synthetic standards were used for silicate and oxide minerals calibration. Representative data are given in Table 2.

Results

Major and trace elements

The results of the whole-rock major and trace elemental analyses of the samples from the Zhuqing mafic intrusions are presented in Table 1. All the samples in this study have undergone variable degrees of alteration. Although the correlations of

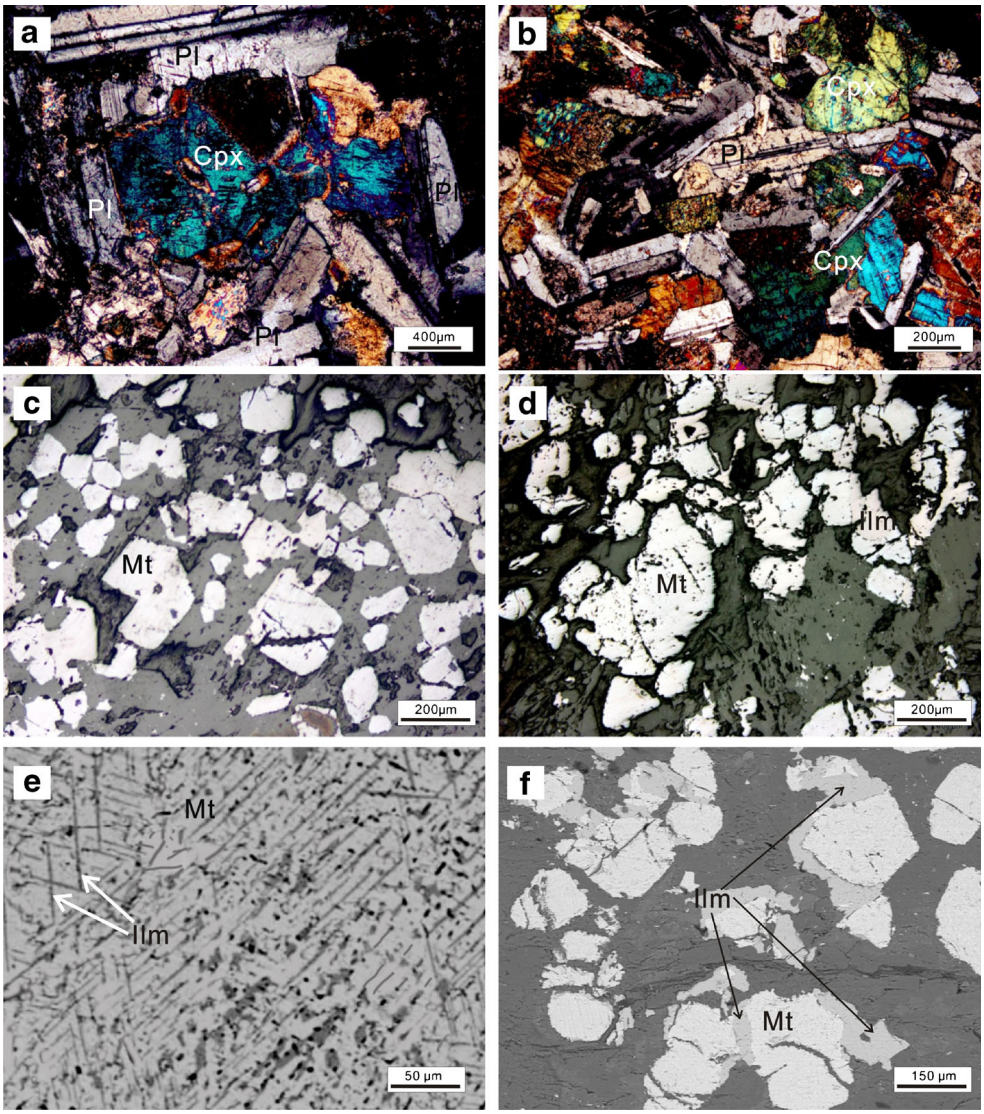

Fig. 3 Microphotographs and BSE images of the gabbros from the Zhuqing intrusions. Microphotographs of **a** sample from lower zone **b** sample from upper zone **c** and **d** the oxide-rich gabbros. BSE images of **e** magnetite with thin trellis type ilmenite exsolutions, and **f** magnetite with coarse ilmenite exsolutions intergrown with magnetite. Pl=plagioclase; Cpx=clinopyroxene; Mt=magnetite; Ilm=ilmenite

major oxides with MgO contents suggest that the effects of alteration on major oxides are minor (Fan et al. 2013), the major oxides described in the following have been recalculated to 100% on a volatile-free base.

The oxide-poor gabbros (Fe_2O_3 < 29 wt.%) of the Zhuqing intrusions display variable MgO (4.0–6.7 wt.%) and Cr (15–120 ppm) contents, with high Fe_2O_3 (17.9–28.3 wt.%), TiO_2 (4.0–6.3 wt.%) and V (325–801 ppm) contents and low SiO_2 (38.0–45.7 wt.%) contents. The oxide-rich gabbros from the Zhuqing intrusions have relatively higher Fe_2O_3 (29.2–43.6 wt.%), TiO_2 (5.5–10.7 wt.%), MgO (7.8–9.7 wt.%), V (817–2,410 ppm), and Cr (221–895 ppm) contents, but lower SiO_2 (25.4–37.2 wt.%) and Zr (106–151 ppm) contents than those of the ore-barren gabbros (Table 1, Fig. 4). All the samples show evolved compositions with variable Mg# (29.7–36.4) and the MgO, TiO_2, and Cr contents decrease, whereas SiO_2 contents increase upward with stratigraphic height (Fig. 4). Moreover, MgO positively correlates with Fe_2O_3 and TiO_2 and negatively correlates with SiO_2 (Fig. 5).

Chalcophile elements and PGE

Copper and nickel concentrations of all the Zhuqing rocks range from 46 to 144 ppm and 24 to 319 ppm, respectively. Sulfur contents (0.006–0.089 wt.%) in most of the rocks are very low, with the exceptions of four samples collected from the top units of the gabbros having >1,000 ppm S. Cu/Zr ratios of these rocks range from 0.21 to 0.75 with one exception of 1.20. The contents of PGEs in all the analyzed samples are very low and highly variable (total PGEs=1.74–2.74 ppb). The oxide-rich gabbros contain relatively higher Ni (160–319 ppm), Ir (0.067–0.115 ppb), Ru (0.383–1.535 ppb), and Rh (0.071–0.124 ppb) and lower Pt (0.500–0.800 ppb) and Pd (0.481–0.723 ppb) contents than those in the oxide-poor gabbros with

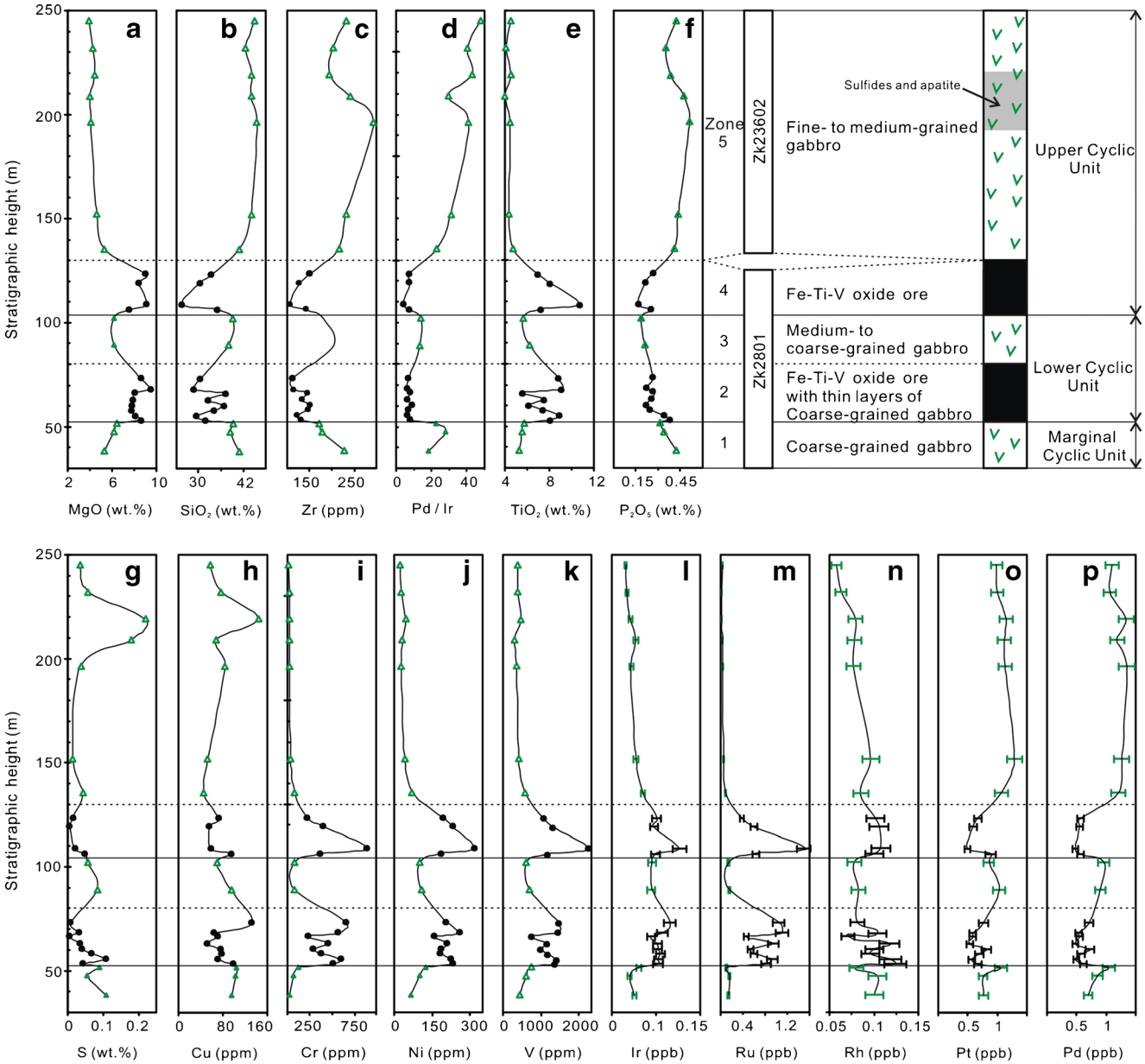

Fig. 4 Variations of MgO, SiO_2, Zr, Pd/Ir, TiO_2, P_2O_5, S, Cu, Cr, Ni, V, Ir, Ru, Rh, Pt and Pd across a profile through the Zhuqing intrusion

24–125 ppm Ni, 0.023–0.068 ppb Ir, 0.019–0.154 ppb Ru, 0.058–0.104 ppb Rh, 0.759–1.287 ppb Pt, and 0.699–1.345 ppb Pd, respectively. All the gabbros in the Zhuqing intrusions have very high Cu/Pd ratios (3.8×10^4 to 19×10^4) and low Pt/Pd ratios (0.84–1.57, with an average of 1.05). The oxide-poor gabbros exhibit higher Pd/Ir ratios (13.4–47.6) than those of the oxide-rich gabbros (4.2–9.3).

Primitive mantle-normalized Ni, Cu, and PGE values in the Zhuqing intrusions exhibit lower values for Ni, Ir, Ru and Rh relative to Pt, Pd and Cu (Fig. 6). The oxide-poor gabbros have positively-sloped patterns, characterized by significant Ni and PGE depletion and a marked fractionation between Ni–Ir and Ru (especially Ru). It is notable that the rocks from zone 5 show negative Ru anomalies (Fig. 7d). The oxide-rich gabbros also have positively-sloped patterns similar to those of the oxide-poor gabbros except for the obvious Ru enrichments relative to Ir and Rh, higher Ir–Ru, Ni and lower Pt–Pd,resulting in the flatter patterns of the oxide-rich gabbros than those of the oxide-poor gabbros.

PGEs in all samples from the Zhuqing intrusions show good correlations with each other. The Ir and Rh contents correlate positively with Ru contents, whereas Pt and Pd contents correlate negatively with Ru contents (Fig. 7). Meanwhile, the Pt contents correlate positively with Pd contents in the Zhuqing gabbros (Fig. 7). Vanadium contents of these rocks exhibit good correlations with Ir, Ru,

Table 1 Concentrations of major oxides (wt. %), trace elements (ppm), S (wt. %) and PGE (ppb) of gabbros and ore samples from the Zhuqing intrusions

Sample No.	ZK2834	ZK2830	ZK2827	ZK2826	ZK2825	ZK2823	ZK2822	ZK2821	ZK2818	ZK2817	ZK2816	ZK2810
Rock name	Gab	Gab	Gab	Ore	Ore	Ore	Ore	Ore	Ore	Ore	Ore	Gab
Drill core	ZK2801	ZK2801	ZK2801	ZK2801	ZK2801	ZK2801	ZK2801	ZK2801	ZK2801	ZK2801	ZK2801	ZK2801
Stratigraphic height/m	38.3	47.5	51.6	53.2	55.3	58.0	60.2	62.9	66.4	68.1	73.2	89.1
Zone	1	1	1	2	2	2	2	2	2	2	2	3
SiO_2	40.00	37.00	38.00	31.00	28.50	33.00	35.75	31.46	35.88	27.85	29.37	36.93
TiO_2	5.16	5.36	5.56	7.88	8.60	7.17	5.97	7.31	5.35	8.86	8.58	6.07
Al_2O_3	11.39	11.88	12.01	8.82	7.49	10.34	10.79	9.28	10.77	6.32	6.87	10.39
Fe_2O_3	24.90	25.03	24.95	33.01	36.50	30.86	28.70	33.02	28.14	39.51	36.81	27.49
MnO	0.32	0.29	0.27	0.33	0.40	0.30	0.30	0.38	0.29	0.51	0.43	0.34
MgO	5.33	6.19	6.45	8.62	8.05	7.75	7.86	7.95	8.06	9.46	8.57	6.21
CaO	6.19	6.34	5.72	6.00	5.82	5.30	4.65	5.19	4.01	4.65	4.71	6.39
Na_2O	2.58	2.29	2.25	0.22	0.17	1.09	1.48	0.81	1.26	0.14	0.28	1.84
K_2O	1.67	1.46	1.39	1.44	1.04	1.37	1.45	1.58	2.44	0.20	1.42	1.12
P_2O_5	0.41	0.33	0.30	0.24	0.21	0.24	0.27	0.21	0.25	0.21	0.18	0.37
L.O.I	1.97	3.65	3.06	2.50	2.28	2.62	2.60	2.23	2.83	2.32	1.73	2.44
Total	99.92	99.82	99.96	100.06	99.06	100.04	99.82	99.42	99.28	100.03	98.95	99.59
$Mg^{\#}$	29.8	32.9	33.9	34.1	30.4	33.2	35.2	32.3	36.2	32.2	31.6	30.9
Y	37.8	29.0	28.1	21.5	18.6	22.4	24.7	18.7	24.9	16.1	19.3	32.8
Zr	228	178	171	131	122	147	151	133	145	114	111	204
Nb	38.5	29.7	30.4	24.2	22.4	25.9	27.6	22.5	24.0	20.8	22.9	35.0
V	482	656	801	1470	1520	1260	1030	1240	817	1560	1580	739
Cr	27.0	68.0	120	514	602	382	289	464	237	574	668	80
Ni	66.0	103	125	232	227	183	188	210	160	260	208	107
Cu	96.5	103.0	104.7	98.4	71.5	77.6	77.0	52.1	71.2	63.6	133.0	94.9
S	0.108	0.055	0.089	0.043	0.108	0.069	0.040	0.034	0.006	0.032	0.008	0.084
Ir	0.038	0.031	0.046	0.078	0.079	0.083	0.078	0.077	0.067	0.086	0.099	0.067
Ru	0.14	0.15	0.11	0.82	0.93	0.60	0.54	0.94	0.46	1.10	1.04	0.15
Rh	0.10	0.10	0.080	0.12	0.12	0.096	0.10	0.12	0.071	0.10	0.08	0.082
Pt	0.77	0.76	1.06	0.67	0.57	0.69	0.81	0.53	0.59	0.59	0.77	1.03
Pd	0.70	0.85	1.04	0.61	0.49	0.57	0.72	0.48	0.55	0.54	0.71	0.90
Sample No.	ZK2806	ZK2805	ZK2804	ZK2802	ZK2801	ZK3601	ZK3603	ZK3606	ZK3609	ZK3614	ZK3627	ZK3629
Rock name	Gab	Ore	Ore	Ore	Ore	Gab	Gab	Gab	Gab	Gab	Gab	Gab
Drill core	ZK2801	ZK2801	ZK2801	ZK2801	ZK2801	ZK3602	ZK3602	ZK3602	ZK3602	ZK3602	ZK3602	ZK3602
Stratigraphic height/m	102.2	106.3	108.9	119.1	123.4	135.5	152.0	196.5	209.0	219.0	232.0	245.0
Zone	3	4	4	4	4	5	5	5	5	5	5	5
SiO_2	38.07	33.83	24.84	29.17	32.16	40.06	43.17	44.71	43.18	43.26	41.62	44.16

Table 1 (continued)

TiO_2	5.53	6.98	10.49	7.77	6.67	4.652	4.264	4.386	3.895	4.437	4.045	4.423
Al_2O_3	12.14	10.20	5.31	7.14	8.99	12.54	12.82	13.31	13.76	13.29	13.33	14.01
Fe_2O_3	25.50	29.85	42.55	36.97	31.41	21.95	19.62	17.85	20.10	18.66	21.12	17.52
MnO	0.31	0.27	0.45	0.38	0.30	0.242	0.234	0.261	0.205	0.247	0.203	0.224
MgO	6.17	7.56	9.09	8.45	9.08	5.29	4.60	4.10	3.99	4.46	4.28	3.88
CaO	5.19	5.23	4.37	4.72	4.95	6.76	6.29	6.75	4.80	7.17	6.26	7.00
Na_2O	2.63	1.01	0.23	0.29	0.14	2.27	2.98	3.89	3.06	3.19	2.73	3.63
K_2O	1.40	1.73	0.12	1.02	2.57	2.21	2.20	1.07	3.17	1.85	2.36	1.16
P_2O_5	0.33	0.25	0.16	0.20	0.26	0.401	0.422	0.497	0.462	0.375	0.346	0.412
L.O.I	2.58	2.53	1.36	3.08	3.14	2.18	2.16	2.16	2.15	1.92	2.42	2.64
Total	99.85	99.44	98.97	99.19	99.67	98.56	98.77	98.99	98.78	98.87	98.70	99.05
Mg#	32.4	33.4	29.7	31.2	36.4	32.3	31.7	31.3	28.2	32.1	28.6	30.5
Y	28.4	23.2	17.9	19.7	25.6	37.8	39.8	43.2	39.2	34.1	32.4	36.7
Zr	181	143	106	128	148	216	232	294	241	195	203	233
Nb	30.2	26.5	20.3	22.4	24.5	40.0	41.2	48.5	41.8	36.2	34.0	40.0
V	660	1250	2410	1410	1130	618	439	379	325	495	423	422
Cr	81.0	376	895	405	221	78.1	35.9	24.2	22.9	18.7	19.8	15.0
Ni	103	185	319	234	196	71.2	40.9	27.9	33.0	46.2	28.0	24.1
Cu	69.6	96.0	58.3	56.3	73.0	45.9	52.7	83.6	67.1	144	77.4	56.6
S	0.056	0.050	0.021	0.006	0.015	0.043	0.013	0.037	0.179	0.221	0.058	0.035
Ir	0.068	0.075	0.12	0.072	0.076	0.052	0.041	0.033	0.040	0.031	0.026	0.023
Ru	0.14	0.64	1.54	0.59	0.38	0.085	0.046	0.044	0.039	0.019	0.020	0.031
Rh	0.078	0.10	0.11	0.11	0.10	0.085	0.097	0.077	0.079	0.079	0.063	0.058
Pt	0.86	0.88	0.50	0.59	0.67	1.07	1.29	1.13	1.11	1.15	1.00	0.99
Pd	0.96	0.56	0.48	0.55	0.56	1.20	1.27	1.35	1.19	1.34	1.06	1.10

Mg#=100*molar MgO/(Mg+FeO_T), assuming FeO_T=0.9*Fe_2O_3, Total iron as FeO_T, Gab=Fe-Ti-V oxide-poor gabbro; Ore=Fe-Ti-V oxide-rich gabbro

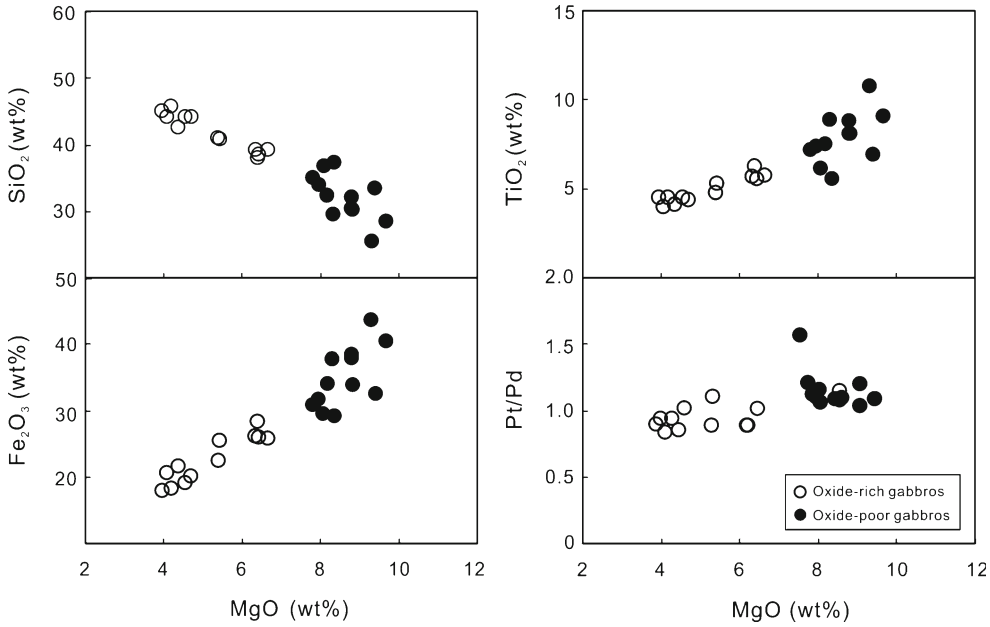

Fig. 5 Plots of MgO versus SiO_2 (**a**), Fe_2O_3 (**b**), TiO_2 (**c**), and Pt/Pd (**d**) for the Zhuqing gabbros

Rh, Cr, and Ni contents (Figs. 4 and 8). However, sulfur contents correlate poorly with PGE contents (Figs. 4 and 9). Zirconium as an incompatible element shows positive correlations with Y, Pt and Pd, and negative correlations with Ir, Ru and Rh (Fig. 10).

Variations in Ni, Cu, S, and PGE concentrations of the rocks along the drill cores are shown in Fig. 4. Ni, Ir, Ru, and Rh contents decrease whereas Cu, S, Pt, and Pd contents and Pd/Ir ratios increase from the base upward within each of the cycle units.

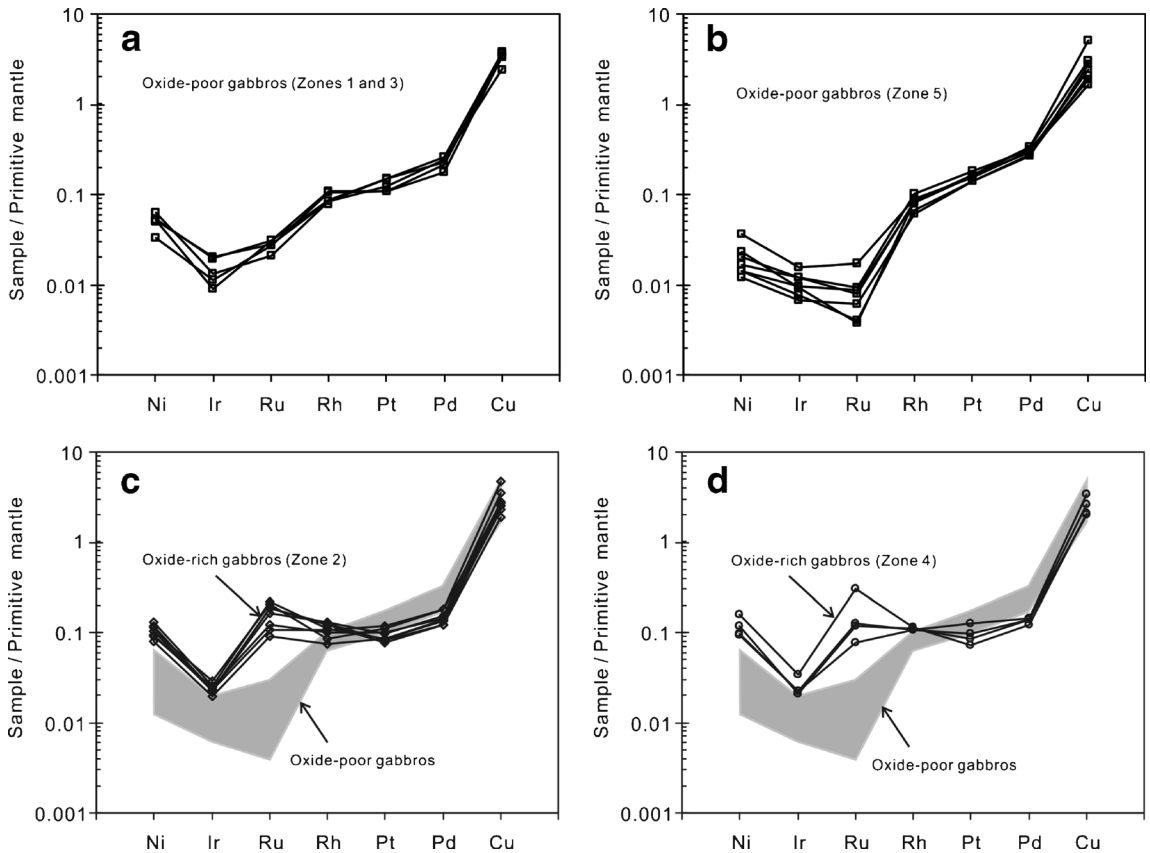

Fig. 6 Primitive mantle-normalized Cu, Ni, and PGE patterns for gabbros from different zones in the profile (see Fig. 4) of the Zhuqing intrusions (normalization factors from Barnes and Maier 1999)

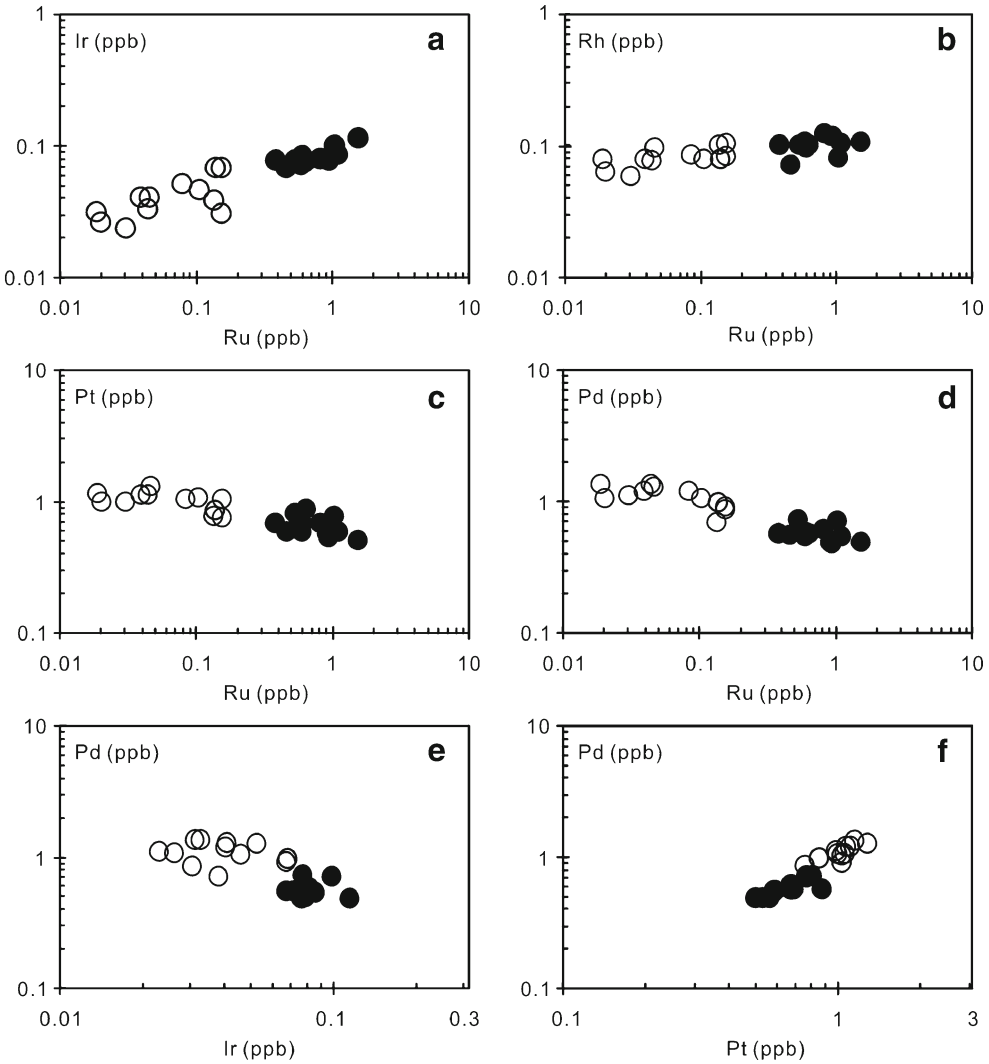

Fig. 7 Plots of Ru versus Ir (**a**), Rh (**b**), Pt (**c**), Pd (**d**) and Ir versus Pd (**e**) and Pt versus Pd (**f**) for the Zhuqing gabbros, showing positive correlations between Ir, Rh and Ru, and between Pt and Pd, and negative correlations between Pt, Pd and Ru, and between Pd and Ir. Symbols as in Fig. 5

Compositions of magnetite

Magnetites in the Zhuqing gabbros have a wide range in composition (Table 2). The magnetites contain 8.86 to 30.21 wt.% TiO_2, and up to 0.06 wt.% MgO. Variable Ti contents are likely caused by ilmenite exsolutions within the magnetites. Higher Ti contents were detected where larger ilmenite exsolutions are lacking within magnetites. Lower and more variable Ti contents are found in granins/microareas where variable amounts of coarse ilmenite exsolutions are present and exsolution of Ti from magnetite is more advanced Magnetites in the oxide-rich gabbros generally have relatively higher FeO, V_2O_3, and Cr_2O_3 contents and lower Fe_2O_3 contents than those in the oxide-poor gabbros. V_2O_3 and Cr_2O_3 contents vary from 0.22 to 1.17 wt.% and from 0.01 to 0.45 wt.% for magnetites in the oxide-rich and oxide-poor gabbros, respectively. Moreover, the positive correlations between Cr and V in whole-rock compositions and V_2O_3 versus Cr_2O_3 contents in magnetite compositions are consistent with the compatible behavior of Cr and Ni into magnetite ($D_{Cr}^{Mt/liq}$=153, Rollinson 1993; $D_{Ni}^{Mt/liq}$=31–65, Nielsen 1992) (Fig. 11), suggesting that the higher Cr contents of the oxide-rich gabbros relative to the oxide-poor gabbros are not only because the oxide-rich gabbros contain more magnetite but also because magnetite is richer in Cr contents.

Discussion

PGE behavior during the evolution of the Zhuqing magma

Chalcophile elements such as Ni, Cu and PGE strongly partition into sulfide liquid due to the high partition coefficients between sulfide and silicate liquids (10^4–10^5 for PGE: Stone et al. 1990; Bezmen et al. 1994; Peach et al. 1994; Fleet et al. 1996; Crocket et al. 1997 or ~10^7–10^{11} for PGE: Fonseca et al. 2009; 10^2–10^3 for Cu and Ni: Rajamani and Naldrett 1978; Francis 1990; Peach et al. 1990; Gaetani and Grove 1997). The distribution of PGE in mafic and ultramafic rocks is therefore most commonly controlled by magmatic sulfides, PGMs and to a lesser extent by oxides (chromite) and silicates (olivines; e.g., Barnes et al. 1985).

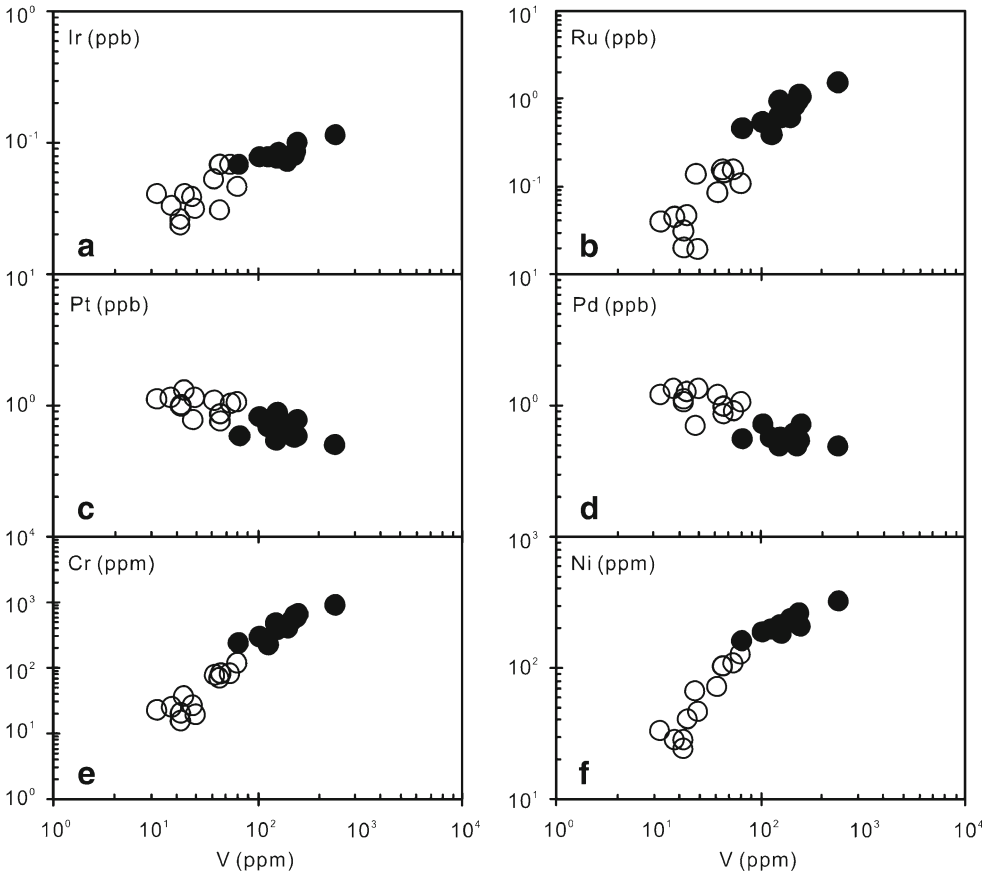

Fig. 8 Plots of V versus PGE (**a**–**d**), Cr (**e**) and Ni (**f**) for the Zhuqing gabbros, showing positive correlations between V and Ir, Ru, Cr and Ni contents. Symbols as in Fig. 5

Traditionally, PGEs have been considered to be immobile, but their immobility has been debated. For example, hydrothermal PGE mineralization has been proposed for the Cu-Ni sulfides at Rathbun Lake, northeastern Ontario (Rowell and Edgar 1986) and for the New Rambler mine in Wyoming (McCallum et al. 1976). Palladiuim has been found to be more mobile than Pt during different types of syn- to post-magmatic hydrothermal alteration (e.g., Li and Naldrett 1993), lower temperature alteration and serpentinization (e.g., Prichard et al. 2001; Seabrook et al. 2004) and weathering (e.g., Fuchs and Rose 1974; Prichard and Lord 1994).

Good positive correlations between Ir and Ru and between Pt and Pd, but depletion of IPGE (Ir, Ru) compared to PPGE (Pt, Pd) in the Zhuqing mafic intrusions (Figs. 6 and 7), indicate that originally PGEs have not been affected by alteration. Moreover, Pt/Pd ratios of most rocks are ~1 together with a positive correlation of Pt and Pd (Fig. 7f). This indicates a coherent behavior of these elements during the magma evolution to form the Zhuqing gabbros and the generally immobile nature of Pd during hydrothermal alteration.

The weak correlations between S and PGEs in the Zhuqing gabbros (Figs. 4 and 9) could be the result of (1) involvement of sulfide liquids having highly variable Cu and PGE concentrations or (2) loss of S via sulfide-oxide re-equilibration on cooling (Naldrett et al. 2012) or post-magmatic hydrothermal alteration (see examples given by Li et al. 2004, 2008). The first possibility is rejected in view of the fact that Ir and Ru and Pt and Pd are positively correlated in the samples (Fig. 7). Loss of S caused by sulfide-oxide re-equilibration or hydrothermal alteration often results in the formation of secondary PGMs (e.g., Wang et al. 2008). However, no such PGMs were detected in the studied sections, which is consistent with the extremely low total PGE contents of these rocks. Hence, a decoupling of PGE and S caused by the loss of S can be ruled out and sulfide liquid may be not have been the only collector of PGE at Zhuqing.

Control of PGEs by magnetite

The whole-rock V concentrations exhibit good correlations with Ir, Ru, and Rh (Fig. 8), suggesting that magnetite is likely the dominant phase that controls Ir, Ru, and Rh distribution. Similar to the distribution of IPGE (Ir and Ru) tending to be enriched in chromite (e.g., Pagé et al. 2012 and references therein), Ir, Ru and Rh in the studied magnetite-rich rocks could either be present in solid solution in the magnetite structure or could be controlled by PGMs (e.g., inclusions of laurite or other PGE alloys) closely associated with magnetite crystallization. Laser ablation inductively coupled plasma mass spectrometry (LA–ICP–MS) can be used to determine whether Ir, Ru and Rh are present in magnetite, what was tried on the Zhuqing samples.

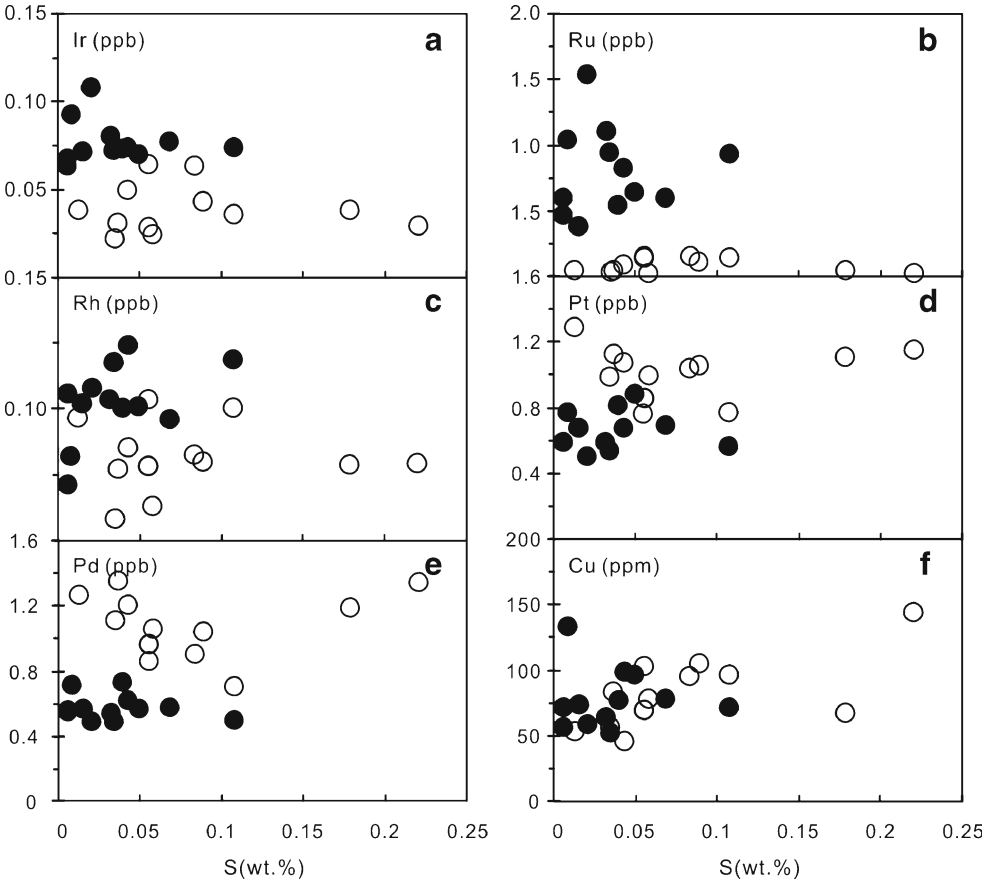

Fig. 9 Plots of S versus PGE (**a**-**e**) and Cu (**f**). Symbols as in Fig. 5

However, the PGE concentrations in the Zhuqing magnetites were always below the detection limits (see analytical method and detection limits for the IPGEs given by Pagé et al. 2012). Pagé et al. (2012) recently analyzed chromite with LA–ICP–MS and found that the IPGEs do not occur in solid solution in chromite but were incorporated in laurite that co-crystallized with the cogenetic chromite. However, in our samples no PGMs have been identified within the sections likely due to the very low total PGE contents of these rocks. Thus, in the Zhuqing gabbros Ir, Ru, and Rh are likely hosted in magnetite rather than in distinct PGMs..

Due to the selective concentration of PGEs by magnetite, Ir, Ru, and Rh behave as compatible elements whereas Pt and Pd behave as incompatible elements in magnetite of the Zhuqing gabbros (Figs. 4 and 9). Hence, magnetite in the Zhuqing intrusions relatively concentrated Ir, Ru and Rh in preference to Pt and Pd. In addition, fractional crystallization of magnetite has contributed to the obviously different contents of Ir–Ru–Rh and Pt–Pd between the oxide-rich gabbros and the oxide-poor ones in the Zhuqing intrusions (Figs. 4 and 6).

The IPGEs behave as compatible elements in many mafic magma systems and it is commonly suggested that they partition into spinels (e.g., Capobianco et al. 1994; Righter 2001). Capobianco et al. (1994) determined the partition coefficients of Ru, Rh and Pd into magnetite and found that Ru and Rh have high partition coefficients (20–1,000), whereas Pd is incompatible with magnetite. Furthermore, the experiments by Brenan et al. (2012) also indicated that IPGE (especially Ru) strongly partition into spinel, with partition coefficients of 4–35 (D_{Ru}) between spinel and magma. In contrast, Pt and Pd are incompatible in the spinel structure and their abundances increase in the fractionated magma during spinel crystallization. IPGEs in the Upper Zone of the Bushveld Complex appear to be controlled by Fe-Ti oxides (Harney et al. 1990; Barnes et al. 2004). Therefore, magnetite may also concentrate Ir, Ru, and even Rh in the same way as proposed for chromite (Pagé et al. 2012), which, as discussed earlier, has been confirmed by PGE behavior in the Zhuqing gabbros.

Fractionation of PGEs during magnetite crystallization

The compatible behavior of the elements Ir and Ru during mafic magma crystal fractionation is well documented (e.g., Barnes et al. 1985; Barnes and Picard 1993; Wyman et al. 1995). Experiments have confirmed that there is only a slight difference in partition coefficients of individual PGE between sulfide and silicate melts (e.g., Bezmen et al. 1994; Peach et al. 1994; Fleet et al. 1996). Thus, removal of sulfide liquid from magma cannot explain the steeply positively-sloped primitive mantle-normalized patterns for the gabbros (Fig. 6). However, IPGEs

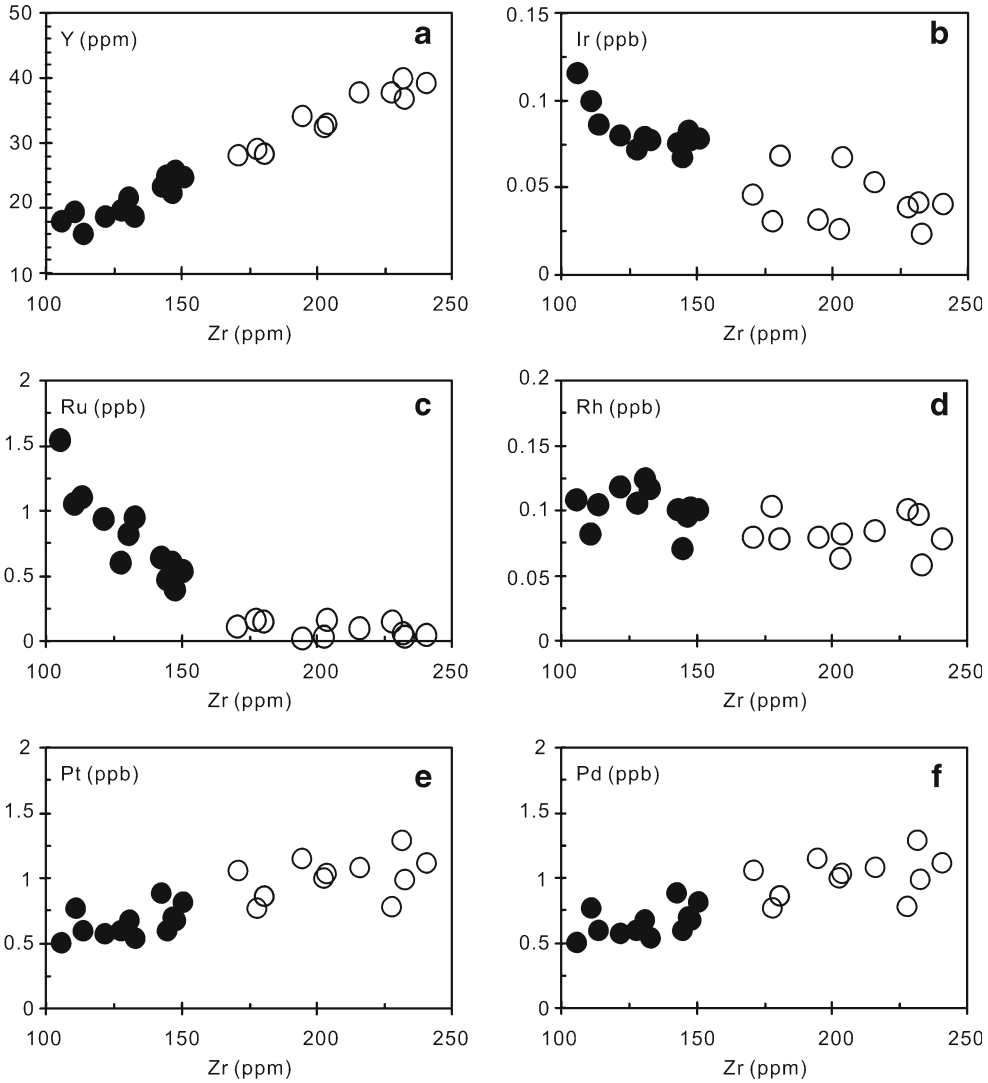

Fig. 10 Plots of Zr versus Y (**a**), Ir (**b**), Ru (**b**), Rh (**c**), Pt (**c**) and Pd (**d**) for the Zhuqing rocks. Symbols as in Fig. 5

are more compatible than PPGEs (Rh, Pt, and Pd) in chromite and may fractionate from each other during fractional crystallization of chromite in mafic magmas (Barnes and Picard 1993; Peach and Mathez 1996; Puchtel and Humayun 2001; Brenan et al. 2003, 2005, 2012; Righter et al. 2004). Therefore, the overall depletion of Ir and Ru over Pt and Pd and the increase of Pd/Ir ratios in these samples may also be due to the removal of chromite from the primary magma, whereas the depletion of Ni relative to Cu can be explained by the removal of olivine during ascent through the crust, prior to emplacement of the Zhuqing intrusions, because olivine preferentially concentrates Ni (Barnes et al. 1985; Keays 1995).

The Ru anomalies in basalts, ultramafic rocks and chromitites have been documented elsewhere in the world, such as, the negative Ru anomalies in basalts (e.g., Philipp et al. 2001; Chazey and Neal 2005; Qi and Zhou 2008) and the positive Ru anomalies in chromites (Büchl et al. 2004) from dunites and harzburgites (Lorand et al. 2004), and komatiites (Fiorentini et al. 2004). Qi and Zhou (2008) suggested that positive Ru anomalies in olivine and chromite and negative Ru anomalies in basalts may reflect removal of laurite in the primary magma, followed by coprecipitation with chromian spinel, olivine or sulfide fractionation. However, removal of sulfide melts from magmas cannot explain such negative Ru anomalies because individual PGE exhibit similar behavior between sulfide and silicate melts (e.g., Bezmen et al. 1994; Peach et al. 1994; Fleet et al. 1996). The Ru anomalies in the Zhuqing oxide-rich gabbros therefore may be due to the higher compatibility of Ru relative to Ir and Rh in magnetite and variable magnetite concentrations in the rocks.

To evaluate the approximate degree of compatibility of PGEs in the Zhuqing gabbros, Spearman correlations and regression lines between individual PGE were calculated (Table 3). The calculations are based on the entire set of 24 gabbros from the Zhuqing intrusions. The slope of the regression line between two different PGEs is a measure of the difference in their compatibility. If the compatibility of Ru is taken as one, compatibility factors for the other PGEs are calculated to be 0.024 for Rh and 0.047 for Ir, whereas Pt and Pd are incompatible in the Zhuqing

Table 2 Average compositions of magnetite in gabbros from the Zhuqing intrusions calculated from n EMPA analyses. Fe^{3+} and Fe_2O_3 calculated assuming 4 oxygens and 3 cations per formula unit

Sample No.	ZK2834	ZK2830	ZK2827	ZK2825	ZK2823	ZK2822	ZK2821	ZK2818	ZK2817	ZK2816	ZK2806	ZK2805	ZK2804	ZK2802	ZK2801
Rock name	Gab	Gab	Gab	Ore	Ore	Ore	Ore	Ore	Ore	Ore	Gab	Ore	Ore	Ore	Ore
Drill core	Zk2801														
Unit	1	1	1	2	2	2	2	2	2	2	3	4	4	4	4
n	4	5	3	2	8	7	6	1	2	5	5	2	4	8	7
MgO	0.02	0.02	0.04	0.02	0.01	0.02	0.04	0	0.05	0.01	0.02	0.01	0.02	0.03	0.03
Al_2O_3	0.01	0.01	0.06	0.02	0.03	0.04	0.03	0.04	0.03	0.04	0.03	0.03	0.03	0.06	0.04
TiO_2	30.21	19.64	20.65	13.97	17.77	19.69	18.24	8.86	12.67	14.25	24.63	21.34	17.47	8.90	22.62
FeO	56.52	47.82	48.3	42.79	46.27	47.99	46.78	38.92	42.11	43.6	51.84	49.87	46.32	38.75	51.18
Fe_2O_3	9.91	30.33	27.39	39.84	33.07	29.36	32.10	50.83	42.64	40.00	20.50	27.06	32.88	49.78	24.47
V_2O_3	0.22	0.43	0.47	0.84	0.67	0.62	0.81	0.69	1.12	0.80	0.39	0.58	1.17	1.03	0.71
MnO	2.32	1.33	1.35	0.76	0.94	0.99	0.95	0.36	0.47	0.56	1.84	0.98	0.63	0.31	0.84
Cr_2O_3	0.01	0.04	0.05	0.29	0.19	0.17	0.30	0.26	0.31	0.34	0.03	0.07	0.45	0.37	0.09
Total	99.22	99.61	98.30	98.53	98.96	98.90	99.25	99.95	99.38	99.60	99.28	99.94	98.97	99.22	99.98
Mg	0.001	0.001	0.002	0.001	0.001	0.001	0.002	0.000	0.003	0.001	0.001	0.001	0.001	0.002	0.002
Al	0.000	0.000	0.003	0.001	0.001	0.002	0.001	0.002	0.001	0.002	0.001	0.001	0.001	0.002	0.002
Ti	0.849	0.547	0.582	0.391	0.497	0.551	0.508	0.245	0.350	0.395	0.689	0.592	0.485	0.247	0.626
Fe^{2+}	1.765	1.481	1.515	1.332	1.438	1.494	1.448	1.195	1.295	1.344	1.613	1.538	1.432	1.194	1.575
Fe^{3+}	0.297	0.901	0.824	1.189	0.985	0.876	0.952	1.497	1.257	1.182	0.612	0.800	0.974	1.471	0.722
V	0.014	0.027	0.030	0.053	0.042	0.039	0.051	0.043	0.069	0.050	0.025	0.036	0.073	0.064	0.044
Mn	0.073	0.042	0.043	0.024	0.030	0.031	0.030	0.011	0.015	0.017	0.058	0.031	0.020	0.010	0.026
Cr	0.000	0.001	0.001	0.009	0.006	0.005	0.009	0.008	0.009	0.010	0.001	0.002	0.013	0.011	0.003
Total	3.000	3.000	3.000	3.000	3.000	3.000	3.000	3.000	3.000	3.000	3.000	3.000	3.000	3.000	3.000

Gab=Fe-Ti-V oxide-poor gabbro; Ore=Fe-Ti-V oxide-rich gabbro; n=number of analysis

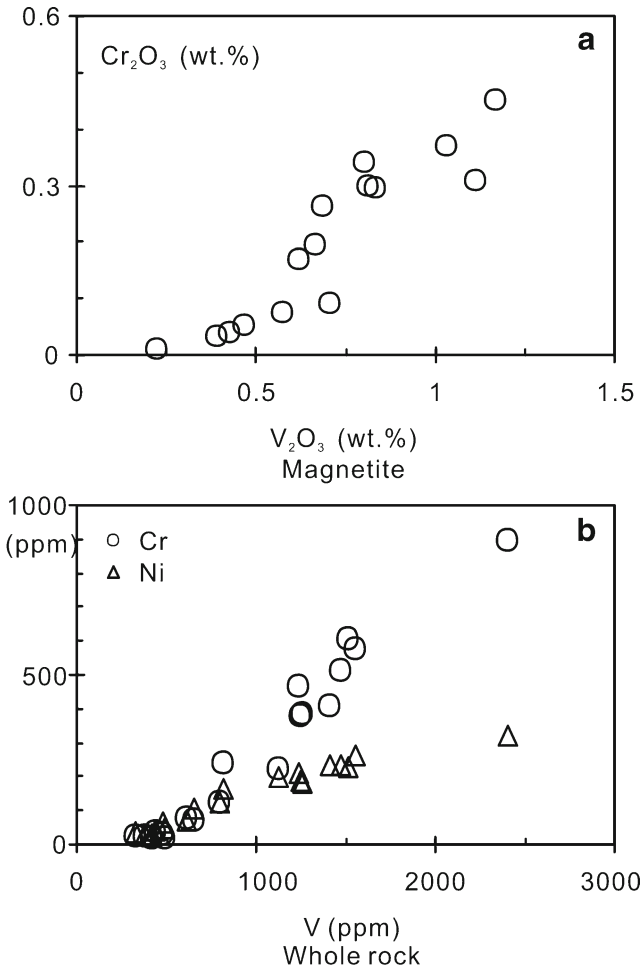

Fig. 11 Plots of V_2O_3 versus Cr_2O_3 in magnetite, and whole-rock V versus Cr and Ni for the Zhuqing gabbros

gabbros. In addition, Pd is 1.22 times more incompatible than Pt. Hence, the order of relative incompatibility as shown by the Zhuqing gabbros under investigation appears to be Pd < Pt < Rh < Ir < Ru. Magnetites concentrating Ir, Ru and Rh crystallized and settled to the lower sections of the magma chamber, thereby resulting in a rapid decrease of these elements in the residual melts (Fig. 4). Thus, the fractionation between Ir–Ru–Rh and Pt–Pd in the Zhuqing gabbros was mainly attributed to fractional crystallization of chromite at depth and magnetite in the upper zone, whereas Ru anomalies are mainly due to variable degrees of PGE compatibility. Meanwhile, Pt and Pd increase following fractional crystallization due to their incompatible behavior (Fig. 4). Pd behaved more incompatibly than Pt and thus resulted in decreasing Pt/Pd ratios with decreasing MgO contents (Fig. 5). However, Pt/Pd ratios of the Zhuqing gabbroic rocks (mean of 1.0, see Table 1) are lower than that of primitive mantle (~1.4; Barnes and Maier 1999) and could be inherited from a mantle source with lower Pt/Pd ratios and/or from a primary magma generated by small degrees of mantle melting because Pd is more chalcophile than Pt (Vogel and Keays 1997) and therefore will be preferentially melted into sulfide saturated magma.

Table 3 Spearman correlation coefficients (r) with significance levels (S_r), slopes (b) and intercepts (a) of regression lines with standard errors (S_b and S_a; 1 sigma) for PGE concentrations in the Zhuqing gabbros

X	Y	r	s_r	b	s_b	a	s_a
Pt	Pd	0.9456	3.42×10^{-14}	1.22	0.087	−0.20	0.075
Pt	Ir	0.6116	5.44×10^{-04}	−0.072	0.017	0.12	0.014
Ru	Pt	0.7297	1.05×10^{-05}	−0.37	0.073	0.96	0.040
Ru	Ir	0.7938	4.64×10^{-07}	0.047	0.007	0.042	0.004
Ru	Rh	0.6247	3.80×10^{-04}	0.024	0.007	0.082	0.004

PGE depletion and low degree of partial melting

It is inappropriate to determine whether sulfur saturation occurred in the Zhuqing gabbros because sulfur analyses of the present samples likely would not yield the original composition prior to degassing due to the possible sulfur loss (e.g., Bai et al. 2012a and references therein). However, it is possible to judge the S-saturation state from the behavior of incompatible trace elements such as Cu, Zr, and the PGEs. Generally, S-saturated magmas would be depleted in PGEs due to the high partition coefficients into sulfide liquid, resulting in a high Cu/Pd ratio of the residual magma. Both Cu and Zr are highly incompatible in S-undersaturated mafic magmas. However, Cu is highly chalcophile whereas Zr is highly lithophile in S-saturated mafic magmas. If the rocks had undergone sulfide liquid removal from magmas, the rocks that formed from the magmas should have lower Cu/Zr ratios. All the rocks in the Zhuqing gabbros have much lower PGE contents and Cu/Zr ratios and much higher Cu/Pd ratios than those in the S-undersaturated and PGE-undepleted mafic–ultramafic rocks in the Bushveld Complex (Harney et al. 1990) and the Rio Jacaré intrusion (Sá et al. 2005), and in basaltic suites from the Siberian Traps and the East Greenland continental flood basalt (CFB) (Momme et al. 2002). Thus, the parental magma of the Zhuqing rocks is significantly depleted in PGE and was likely S-saturated.

PGE concentrations of a primary magma depend on the degree of partial melting and sulfur concentration of the mantle source. Partial melting of the primitive mantle may lead to the formation of either S-saturated or S-undersaturated magmas. Mantle-derived magmas are commonly S-saturated at low degrees of partial melting, although they can be S-undersaturated under high fO_2 (e.g., Jugo et al. 2005; Mungall et al. 2006). If the melts derived from the mantle source were S-saturated, the immiscible sulfide liquids would have stayed in the residual mantle, resulting in PGE-poor magma. It has been proposed that the Zhuqing gabbros were probably derived from low degrees of partial melting of a mantle source (Fan et al. 2013). Thus, low degree of partial melting of mantle may have led the magma parental to the Zhuqing gabbros to initial S-saturation, whereas the possible removal of sulfide liquid from

the magma during ascent through the crust may not have significantly changed PGE concentrations because the primal magma had already been highly depleted in PGE when the possible sulfide liquid segregation occurred. Sulfide retention in the source mantle has also been proposed to explain PGE depletion in other mafic rocks elsewhere such as the Kiglapait mafic intrusion and the Voisey's Bay intrusion in the Nain Plutonic Suite, Labrador (Lightfoot et al. 2012) and the basalts in the Tarim Basin, northwest China (Li et al. 2012). Magnetite-rich rocks are generally thought to be poor targets for PGE exploration because PGEs have already been removed from the magma by sulfide liquid segregation or PGM crystallization. In contrast, the very low PGE concentrations in the Zhuqing rocks are attributed to low-degree partial melting that left PGEs-rich sulfides behind in the mantle rather than removal of PGEs by subsequent sulfide segregation or PGM crystallization.

Implications for petrogenesis and mineralization

All the samples of the Zhuqing gabbros have MgO contents ranging from 3.96 to 9.68 wt.%, suggesting that the gabbros have undergone a considerable amount of fractional crystallization. This interpretation is supported by the low Ni and Cr contents and high Cu/Ni ratios of these rocks, a feature characteristic of high degrees of fractionation (Lesher and Stone 1996; Lesher and Keays 2002). The rocks from the Zhuqing intrusions have very high Pd/Ir ratios (4.2–47.6), which are typical of highly evolved magma (e.g., Zhou et al. 2005). It is commonly accepted that magnetite and ilmenite crystallize during the late stage in mafic-ultramafic magmas, and late-stage fractional crystallization of titanomagnetite and ilmenite results in the formation of Fe–Ti oxide deposits in the evolved upper parts of layered intrusions, such as the Bushveld Complex (Tegner et al. 2006), the Skaergaard intrusion (McBirney 1996) and the Muskox intrusion (Irvine 1988). However, it had also been suggested that magnetite may crystallize at an early stage from magma with a relatively high fO_2 (Toplis and Carroll 1995; Ganino et al. 2008; Pang et al. 2010; Bai et al. 2012b). However, $D_V^{Mt/liq}$ decreases by approximately one order of magnitude with increasing fO_2 from NNO–0.7 to NNO+2.6 (Canil 1999; Toplis and Corgne 2002), and thus magnetite crystallizing early at high fO_2 conditions is characterized by relatively consistent V_2O_3 contents (Pang et al. 2010; Bai et al. 2012b). The magnetites in all the samples from the Zhuqing Fe–Ti–V oxide ores have obviously higher V_2O_3 contents than those in the oxide-poor gabbros, suggesting a relative high V distribution coefficient between magnetite and silicate melts. Therefore, the fO_2 values were low in the Zhuqing rocks, and it was late-stage fractional crystallization of titanomagnetite and ilmenite from an evolved parental magma that most likely resulted in the formation of Fe–Ti–V oxide deposits in the Zhuqing intrusions.

The Pd/Ir ratios and Pt, Pd, SiO_2, and Zr contents increase whereas Ir, Ru, Cr, Ni, V, MgO, and TiO_2 contents decrease from the base upward in each cyclic unit (Fig. 4) This is consistent with fractional crystallization of the magma from the base to the top, which is further confirmed by good correlations between MgO and major, and trace elements as shown above. Olivine and chromite crystallized during ascent of the magma through the crust and remained in the deeper chamber, leading to the low Ni and low Ir and Ru concentrations in the magma, respectively. Meanwhile, magnetite concentrated Ir, Ru, Cr, Ni and V together with fractional crystallization of clinopyroxene and plagioclase after the evolved Zhuqing magma was emplaced into the upper chamber, resulting in a rapid decrease of Ir, Ru, Cr, Ni, and V contents in the residual melts. Thereafter, ilmenite and magnetite settled to the lower sections of each cyclic unit as a result of the density contrast. The Fe–Ti–V oxide ores exhibit relatively higher Ir, Ru, and Rh contents and positive Ru anomalies due to variously compatible behaviors of Ir, Ru and Rh, whereas the ore-barren gabbros have lower Ir, Ru, and Rh, and elevated Pt and Pd concentrations and negative Ru anomalies (Fig. 5) because magnetite in the ore-barren gabbros crystallized relatively later than that in the ore-bearing ones. Thus, fractional crystallization and cumulative processes are responsible for the formation of the Zhuqing gabbros and magnetite layer in a single cycle.

However, simple fractional crystallization and density sorting of cumulus minerals cannot explain the systemic reversals of geochemical parameters in the different cyclic units. Sharp reversals of major, trace element and trace element ratios (e.g., Pd/Ir, Ni/Cu, and Cu/Pd) (Fig. 4, Table 1) between the boundaries of the cycles indicate that multiple pulses of magma replenishment in the magma chamber may have been involved in the formation of the Zhuqing intrusions. Moreover, a new recharge of more Cr- and V-rich magma is also confirmed by compositional reversals in whole-rock Cr and V contents and by the presence of higher Cr_2O_3 and V_2O_3 in magnetite from the base of each cycle (Table 2). Therefore, both fractional crystallization and multiple magma recharge episodes played important roles in generating the Zhuqing gabbros and the magnetite layers therein.

Conclusions

The following conclusions are drawn from this study:

(1) Magnetite in the Zhuqing gabbros concentrated Ir, Ru, and Rh in preference to Pt and Pd.
(2) The order of relative incompatibility as shown in the Zhuqing gabbros appears to be Pd<Pt<Rh<Ir<Ru. The fractionation between Ir–Ru–Rh and Pt–Pd in the Zhuqing gabbros is mainly attributed to fractional crystallization of early crystallized chromite and later crystallized magnetite, whereas Ru anomalies mainly resulted from variable degrees of compatibility of PGEs with a preference of Ru for the oxides.

(3) The low PGE concentrations and initial sulfur saturation of the magma are mainly attributed to the low degree of partial melting that left sulfides concentrating PGEs behind in the mantle.
(4) The Zhuqing gabbros and magnetite layers were formed by fractional crystallization and multiple episodes of magma recharge.

Acknowledgments We appreciate the assistance of Dr. L. Qi with PGE analysis, Prof. Y. Liu with major element analyses by XRF, Prof. J. Hu, and Ms. G.P. Bao and Y. Huang for trace element analyses by ICP-MS, and Prof. Q. Mao and Y.G. Ma for assistance with EMPA. The paper has benefited from constructive comments of two anonymous reviewers and the chief editor Johann Raith. This work is jointly supported by the 12th 5-Year Plan project of State Key Laboratory of Ore-deposit Geochemistry, Chinese Academy of Sciences (SKLOG-ZY125-06) and the NSFC (Grants 41273049 and 41073043).

Appendix 1

Table 4 Trace element concentrations (in ppm) of international reference materials used for this study

Sample No.	OU-6	AMH-1	GBPG-1
Sc	22.6	14.6	14.4
V	129	112	95.9
Cr	73	43	177
Co	29	19	19
Ni	40	36	57
Cu	40	30	29
Zn	116	71	78
Ga	24.3	19.8	17.8
Rb	123	18.8	53.1
Sr	133	548	336
Y	26.5	15	16.3
Zr	177	146	226
Nb	16	8.84	10.3
Cs	7.95	0.22	0.3
Ba	478	317	853
La	33.00	15.90	48.60
Ce	76.40	32.80	93.60
Pr	7.82	4.15	10.80
Nd	29.40	16.60	38.40
Sm	5.89	3.52	6.07
Eu	1.35	1.10	1.65
Gd	5.19	5.17	4.44
Tb	0.88	0.53	0.62
Dy	4.98	2.78	2.72
Ho	1.11	0.59	0.64
Er	3.05	1.52	1.88
Tm	0.44	0.21	0.27
Yb	2.96	1.37	1.9
Lu	0.46	0.20	0.28
Hf	4.76	3.59	5.52
Ta	1.11	0.59	0.38
Pb	32.4	9.20	13.3
Th	11.4	2.44	10.9
U	1.95	0.82	0.80

Appendix 2

Table 5 Analytical results, blank values and detection limits (DL) of PGE (in ppb) for reference material WGB-1

Elements	Blank		WGB-1			
	Measured	DL	Measured	Qi et al. (2008)	Meisel and Moser (2004)	Certified
Ir	0.0017	0.001	0.16	0.16±0.02	0.21	0.33
Ru	0.0124	0.001	0.12	0.13±0.01	0.14	0.3
Rh	0.0019	0.001	0.22	0.20±0.02	0.23	0.32
Pt	0.0015	0.009	5.39	6.34±0.61	6.39	6.1
Pd	0.0396	0.015	13.84	13.0±1.1	13.9	13.9

Certified=Govindaraju (1994)

References

Bai ZJ, Zhong H, Li C, Zhu WG, Xua GW (2012a) Platinum-group elements in the oxide layers of the Hongge mafic-ultramafic intrusion, Emeishan Large Igneous Province, SW China. Ore Geol Rev 46:149–161

Bai ZJ, Zhong H, Naldrett AJ, Zhu WG, Xu GW (2012b) Whole rock and mineral composition constraints on the genesis of the giant Hongge Fe-Ti-V oxide deposit in the Emeishan Large Igneous Province, SW China. Econ Geol 102:507–524

Barnes S-J, Maier WD (1999) The fractionation of Ni, Cu and the noble metals in silicate and sulphide liquids. In: Keays RR, Lesher CM, Lightfoot PC, Farrow CEG (eds.) Dynamic processes in magmatic ore deposits and their application to mineral exploration. Geological Association of Canada, Short Course Notes Volume 13. pp 69–106

Barnes S-J, Maier WD (2002) Platinum-group elements and microstructures of normal Merensky Reef from Impala Platinum Mines, Bushveld Complex. J Petrol 43:103–128

Barnes S-J, Naldrett AJ, Gorton MP (1985) The origin of the fractionation of platinum-group elements in terrestrial magmas. Chem Geol 53: 303–323

Barnes S-J, Picard CP (1993) The behaviour of platinum-group elements during partial melting, crystal fractionation, and sulphide segregation: an example from the Cape Smith Fold Belt, northern Quebec. Geochim Cosmochim Ac 57:79–87

Barnes S-J, Maier WD, Ashwal LD (2004) Platinum-group element distribution in the Main Zone and Upper Zone of the Bushveld Complex, South Africa. Chem Geol 208:293–317

Bezmen NI, Asif M, Brűgmann GE, Romanenk IM, Naldrett AJ (1994) Distribution of Pd, Rh, Ru, Ir, Os and Au between sulfide and silicate metals. Geochim Cosmochim Ac 58:1251–1260

Brenan JM, McDonough WF, Dalpé C (2003) Experimental constraints on the partitioning of rhenium and some platinum-group elements between olivine and silicate melt. Earth Planet Sci Lett 212:135–150

Brenan JM, McDonough WF, Ash R (2005) An experimental study of the solubility and partitioning of iridium, osmium and gold between olivine and silicate melt. Earth Planet Sci Lett 237:855–872

Brenan JM, Finnigan CF, McDonough WF, Homolova V (2012) Experimental constraints on the partitioning of Ru, Rh, Ir, Pt and Pd between chromite and silicate melt: the importance of ferric iron. Chem Geol 302–303:16–32

Büchl A, Brűgmann G, Batanova VG (2004) Formation of podiform chromitite deposits: implications from PGE abundances and Os isotopic compositions of chromites from the Troodos complex, Cyprus. Chem Geol 208:217–232

Canil D (1999) Vanadium partitioning between orthopyroxene, spinel and silicate melt and the redox states of mantle source regions for primary magmas. Geochim Cosmochim Acta 63:557–572

Capobianco CJ, Hervig RL, Drake MJ (1994) Experiments on Ru, Rh and Pd compatibility for magnetite and hematite solid solutions crystallised from silicate melts. Chem Geol 113:23–44

Chang X, Zhu B, Sun D, Qiu H, Zou R (1997) Isotope geochemistry study of Dongchuan copper deposits in Middle Yunnan Province, SW China: stratigraphic chronology and application of geochemical exploration by lead isotopes. Geochimica 26:32–38 (in Chinese with English abstract)

Chazey WJ, Neal CR (2005) Platinum-group element constraints on source composition and magma evolution of the Kerguelen Plateau using basalts from ODP Leg 183. Geochim Cosmochim Acta 69:685–4701

Crocket JH, Fleet ME, Stone WE (1997) Implications of composition for experimental partitioning of platinum-group elements and gold between sulfide liquid and basalt melt: the significance of nickel content. Geochim Cosmochim Acta 61:4139–4149

Davies G, Tredoux M (1985) The platinum-group element and gold contents of the marginal rocks and sills of the Bushveld complex. Econ Geol 80:838–848

Fan HP, Zhu WG, Li ZX, Zhong H, Bai ZJ, He DF, Chen CJ, Cao CY (2013) Ca. 1.5 Ga mafic magmatism in South China during the break-up of the supercontinent Nuna/Columbia: The Zhuqing Fe-Ti-V oxide ore-bearing mafic intrusions in western Yangtze Block. Lithos 168–169:85–98

Fiorentini ML, Stone WE, Beresford SW, Barley ME (2004) Platinum-group element alloy inclusions in chromites from Archaean mafic-ultramafic units: evidence from the Abitibi and the Agnew-Wiluna Greenstone Belts. Miner Petrol 82:341–355

Fleet ME, Crocket JH, Stone WE (1996) Partitioning of platinum group elements (Os, Ir, Ru, Pt, Pd) and gold between sulfide liquid and basalt melt. Geochim Cosmochim Acta 60:2397–2412

Fonseca ROC, Campbell IH, O'Neill HSC, Allen CM (2009) Solubility of Pt in sulphide mattes: Implications for the genesis of PGE-rich horizons in layered intrusions. Geochim Cosmochim Acta 73:5764–5777

Francis RD (1990) Sulfide globules in mid-ocean ridge basalts (MORB), and effect of oxygen abundance in Fe-S-O liquids on the ability of those liquids to partition metals from MORB and komatiite magmas. Chem Geol 85:199–213

Fuchs WA, Rose AW (1974) The geochemical behavior of platinum and palladium in the weathering cycle in the Stillwater Complex, Montana. Econ Geol 69:332–346

Gaetani GA, Grove TL (1997) Partitioning of moderately siderophile elements among olivine sulfide melt and silicate melt: Constraints on core formation in the Earth and Mars. Geochim Cosmochim Acta 61:1829–1846

Ganino C, Arndt NT, Zhou MF, Gaillard F, Chauvel C (2008) Interaction of magma with sedimentary wall rock and magnetite ore genesis in the Panzhihua mafic intrusion, SW China. Miner Deposita 43:677–694

Gao S, Qiu YM, Ling WL, McNaughton NJ, Groves DI (2001) Single zircon U-Pb dating of the Kongling high-grade metamorphic terrain: Evidence for >3.2 Ga old continental crust in the Yangtze craton. Sci China Ser D 4:326–335

Geng Y, Yang C, Du L, Wang X, Ren L, Zhou X (2007) Chronology and tectonic environment of the Tianbaoshan formation: new evidence from zircon SHRIMP U-Pb age and geochemistry. Geological Rev 53:556–563 (in Chinese with English abstract)

Govindaraju K (1994) 1994 compilation of working values and sample description for 383 geostandards. Geostand Geoanal Res 18:1–158

Greentree MR, Li ZX (2008) The oldest known rocks in south-western China: SHRIMP U-Pb magmatic crystallization age and detrital provenance analysis of the Paleoproterozoic Dahongshan Group. J Asian Earth Sci 33:289–302

Greentree MR, Li ZX, Li XH, Wu H (2006) Late Mesoproterozoic to earliest Neoproterozoic basin record of the Sibao orogenesis in western South China and relationship to the assembly of Rodinia. Precamb Res 151:79–100

Harney DMW, Merkle RKW, Von Gruenewaldt G (1990) Platinum-group element behavior in the lower part of the upper zone, Eastern Bushveld complex; implications for the formation of the main magnetite layer. Econ Geol 85:1777–1789

He DF (2009) Petrological and geochemical characteristics of the Lala copper deposit in Sichuan Province. Unpublished PhD thesis, The Gradute School of the Chinese Academy of Sciences, China, 103 pp (in Chinese with English abstract)

Irvine TN (1988) Muskox intrusion, Northwest Territories. Geological environments of the platinum-group elements. Geol Surv Canada Open File 1440:25–39

Jugo PJ, Luth RW, Richards JP (2005) Experimental data on the speciation of sulfur as a function of oxygen fugacity in basaltic melts. Geochim Cosmochim Acta 69:497–503

Keays RR (1995) The role of komatiitic magmatism and S-saturation in the formation of ore deposits. Lithos 34:1–18

Lesher CM, Keays RR (2002) Komatiite-associated Ni-Cu-(PGE) deposits. In: Cabri LJ (eds.) The geology, geochemistry, mineralogy, mineral beneficiation of the platinum-group elements. Can Inst Mining Metallurgy Pet 54:579–618

Lesher CM, Stone WE (1996) Exploration geochemistry of komatiites. In: Wyman D A (ed.) Igneous trace element geochemical applications for massive Sulphide Exploration. Geological Association of Canada, Short Course Notes 12:153–204

Li C, Naldrett AJ (1993) High chlorine alteration minerals and Ca-rich brines in fluid inclusions from the Strathcona deep copper zone, Sudbury Ontario. Econ Geol 88:1780–1796

Li C, Ripley EM, Merino E, Maier WD (2004) Replacement of base metal sulfides by actinolite, epidote, calcite, and magnetite in the UG2 and Merensky reef of the Bushveld complex, South Africa. Econ Geol 99:173–184

Li ZX, Wartho JA, Occhipinti S, Zhang CL, Li XH, Wang J, Bao CM (2007) Early history of the eastern Sibao orogen (South China) during the assembly of Rodinia: new $^{40}Ar/^{39}Ar$ dating and U–Pb SHRIMP detrital zircon provenance constraints. Precamb Res 159: 74–94

Li C, Ripley EM, Oberthür T, Miller JD, Joslin GD (2008) Textural and stable isotope studies of hydrothermal alteration in the main sulfide zone of the great dyke, Zimbabwe, and the precious metals zone of the Sonju Lake Intrusion, Minnesota, USA. Miner Deposita 43:97–110

Li YQ, Li ZL, Sun YL, Santosh M, Langmuir CH, Chen HL, Yang SF, Chen ZX, Yu X (2012) Platinum-group elements and geochemical

characteristics of the Permian continental flood basalts in the Tarim Basin, northwest China: implications for the evolution of the Tarim Large Igneous Province. Chem Geol 328:278–289

Lightfoot PC, Keays RR (2005) Siderophile and chalcophile metal variations in flood basalts from the Siberian Trap, Noril'sk Region: implications for the origin of the Ni–Cu–PGE sulfide ores. Econ Geol 100:439–462

Lightfoot PC, Keays RR, Evans-Lamswood D, Wheeler R (2012) S saturation history of Nain Plutonic Suite mafic intrusions: origin of the Voisey's Bay Ni–Cu–Co sulfide deposit, Labrador, Canada. Miner Deposita 47:23–50

Lorand JP, Delpech G, Grégoire M, Moine B, O'Reilly SY, Cottin JY (2004) Platinum-group elements and the multistage metasomatic history of Kerguelen lithospheric mantle (South Indian Ocean). Chem Geol 208:195–215

Maier WD (2005) Platinum-group element (PGE) deposits and occurrences: mineralization styles, genetic concepts, and exploration criteria. J Afr Earth Sci 41:165–191

Maier WD, Barnes S-J, Gartz V, Andrews G (2003) Pt-Pd reefs in magnetitites of the Stella layered intrusion, South Africa: a world of new exploration opportunities for platinum group elements. Geology 31:885–888

McBirney AR (1996) The Skaergaard Intrusion. In: Cawthorn RG (ed) Layered intrusions. Elsevier, pp 147–180

McCallum ME, Loucks RR, Carlston RR, Cooley EF, Doerge TA (1976) Platinum metals associated with hydrothermal copper ores of the New Rambler mine, Medicine Bow Mountains, Wyoming. Econ Geol 71: 1429–1450

Momme P, Tegner C, Brooks CK, Keays RR (2002) The behaviour of platinum-group elements in basalts from the East Greenland rifted margin. Contrib Mineral Petrol 143:133–153

Mou CL, Lin SL, Yu Q (2003) The U-Pb ages of the volcanic rock of the Tianbaoshan formation, Huili, Sichuan province. J Stratigr 27:216–219 (in Chinese with English abstract)

Mungall JE, Hanley JJ, Arndt NT, Debecdelievre A (2006) Evidence from meimechites and other low-degree mantle melts for redox controls on mantle-crust fractionation of platinum-group elements. Proc Natl Acad Sci U S A 103:12695–12700

Naldrett AJ, Wilson A, Kinnaird J, Yudovskaya M, Chunnett G (2012) The origin of chromitites and related PGE mineralization in the Bushveld complex: new mineralogical and petrological constraints. Miner Deposita 47:209–232

Nielsen R (1992) BIGD. FOR: a fortran program to calculate trace-element partition coefficients for natural mafic and intermediate composition magmas. Comput Geosci 18:773–788

Pagé P, Barnes S-J, Bédard JH, Zientek ML (2012) In situ determination of Os, Ir, and Ru in chromites formed from komatiite, tholeiite and boninite magmas: Implications for chromite control of Os, Ir and Ru during partial melting and crystal fractionation. Chem Geol 302–303:3–15

Pang KN, Zhou MF, Qi L, Shellnutt JG, Wang CY, Zhao DG (2010) Flood basalt-related Fe-Ti oxide deposits in the Emeishan large igneous province, SW China. Lithos 119:123–136

Peach CL, Mathez EA (1996) Constraints on the formation of platinum-group element deposits in igneous rocks. Econ Geol 91:439–450

Peach CL, Mathez EA, Keays RR (1990) Sulfide melt-silicate melt distribution coefficience for noble metals and other chalcophile elements as deduced from MORB: Implications for partial melting. Geochim Cosmochim Acta 54:3379–3389

Peach CL, Mathez EA, Keays RR, Reeves SJ (1994) Experimentally determined sulfide melt-silicate melt partition coefficients for iridium and palladium. Chem Geol 117:361–377

Philipp H, Eckhardt J-D, Puchelt H (2001) Platinum-group element in basalts of the seaward-dipping reflector sequence, SE Greenland coast. J Petrol 42:407–432

Prichard HM, Lord RA (1994) Evidence for the mobility of PGE in the secondary environment in the Shetland ophiolite complex. Transact Inst Min Metall App Earth Sci 103:B79–B86

Prichard HM, Sà H, Fisher PC (2001) Platinum-group mineral assemblages and chromite composition in the altered and deformed Bacuri Complex, Amapa, northeastern Brazil. Can Mineral 39:377–396

Puchtel IS, Humayun M (2001) Platinum group element fractionation in a komatiitic basalt lava lake. Geochim Cosmochim Acta 65:979–2993

Qi L, Zhou MF (2008) Platinum-group elemental and Sr-Nd-Os isotopic geochemistry of Permian Emeishan flood basalts in Guizhou Province, SW China. Chem Geol 248:83–103

Qi L, Hu J, Grégoire DC (2000) Determination of trace elements in granites by inductively coupled plasma mass spectrometry. Talanta 51:507–513

Qi L, Zhou MF, Wang CY (2004) Determination of low concentrations of platinum group elements in geological samples by ID-ICP-MS. J Ana Atom Spectrom 19:1335–1339

Qi L, Gao JF, Huang XW, Hu J, Zhou MF, Zhong H (2011) An improved digestion technique for determination of platinum group elements in geological samples. J Ana Atom Spectrom 26:1900–1904

Rajamani V, Naldrett AJ (1978) Partitioning of Fe Co Ni and Cu between sulfide liquid and basaltic melts and the composition of Ni-Cu sulfide deposits. Econ Geol 73:82–93

Righter K (2001) Rhenium and iridium partitioning in silicate and magmatic spinels: implications for planetary magmatism and mantles. Lunar and planetary science XXXII:1759

Righter K, Campbell AJ, Humayun M, Hervig RL (2004) Partitioning of Ru, Rh, Pd, Re, Ir, and Au between Cr-bearing spinel, olivine, pyroxene and silicate melts. Geochim Cosmochim Acta 68:867–880

Rollinson H (1993) Using geochemical data: evaluation, presentation, interpretation. Longman Scientific and Technical, pp 108

Rowell WF, Edgar AD (1986) Platinum-group element mineralisation in hydrothermal Cu-Ni sulphide occurrence, Rathbun Lake, northeastern Ontario. Econ Geol 81:1272–1277

Sá JHS, Barnes S-J, Prichard HM, Fisher PC (2005) The distribution of base metals and platinum-group elements in magnetitite and its host rocks in the Rio Jacaré intrusion, Northeastern Brazil. Econ Geol 100:333–348

Seabrook CL, Prichard HM, Fisher PC (2004) Platinum-group minerals in the Raglan Ni-Cu-(PGE) sulfide deposit. Cape Smith, Canada. Can Mineral 42:485–497

Stone WE, Crocket JH, Fleet ME (1990) Partitioning of palladium iridium platinum and gold between sulfide liquid and basalt melt at 1200°C. Geochim Cosmochim Acta 54:2341–2344

Sun WH, Zhou MF, Gao JF, Yang YH, Zhao XF, Zhao JH (2009) Detrital zircon U-Pb geochronological and Lu-Hf isotopic constraints on the Precambrian magmatic and crustal evolution of the western Yangtze Block, SW China. Precamb Res 172:99–126

Tegner C, Cawthorn RG, Kruger FJ (2006) Cyclicity in the main and upper zones of the Bushveld complex, South Africa: crystallization from a zoned magma sheet. J Petrol 47:2257–2279

Toplis MJ, Carroll MR (1995) An experimental study of the influence of oxygen fugacity on Fe-Ti oxide stability, phase relations, and mineral-melt equilibria in ferro-basaltic systems. J Petrol 36:1137–1170

Toplis MJ, Corgne A (2002) An experimental study of element partitioning between magnetite, clinopyroxene and iron-bearing silicate liquids with particular emphasis on vanadium. Contrib Mineral Petr 144:22–37

Vogel DC, Keays RR (1997) The petrogenesis and platinum-group element geochemistry of the Newer Volcanic Province, Victoria, Australia. Chem Geol 136:81–204

Wang CY, Prichard HM, Zhou MF, Fisher PC (2008) Platinum-group minerals from the Jinbaoshan Pd–Pt deposit, SW China: evidence for magmatic origin and hydrothermal alteration. Miner Deposita 43:791–803

Wang LJ, Griffin WL, Yu JH, O'Reilly SY (2013) U-Pb and Lu-Hf isotopes in detrital zircon from Neoproterozoic sedimentary rocks in the northern Yangtze Block: implications for Precambrian crustal evolution. Gondwana Res 23:1261–1272

Wu MD, Duan JS, Song XL, Chen L, Dan Y (1990) Geology of Kunyang Group in Yunnan Province. Scientific Press of Yunnan Province, Kunming, 265 pp (in Chinese with English abstract)

Wyman D, Kerrich R, Sun M (1995) Noble metal abundances of late Archean (2.7 Ga) accretion-related shoshonitic lamprophyres, Superior Province, Canada. Geochim Cosmochim Acta 59:47–57

Yan DP, Zhou MF, Song HL, Wang XW, Malpas J (2003) Origin and tectonic significance of a Mesozoic multi-layer over-thrust within the Yangtze Block (South China). Tectonophysics 361:239–254

Yin FG, Sun ZM, Zhang Z (2011) Mesoproterozoic stratigraphic-structure framework in Huili-Dongchuan area. Geology Review 57:770–778 (in Chinese with English abstract)

Zhang CH, Gao LZ, Wu ZJ, Shi XY, Yan QR, Li DJ (2007) SHRIMP U-Pb zircon age of tuff from the Kunyang group in central Yunnan: evidence for Grenvillian orogeny in south China. Chinese Sci Bull 52: 1517–1525

Zhao XF, Zhou MF (2011) Fe–Cu deposits in the Kangdian region, SW China: a Proterozoic IOCG (iron–oxide–copper–gold) metallogenic province. Miner Deposita 46:731–747

Zhao XF, Zhou MF, Li JW, Sun M, Gao JF, Sun WH, Yang JH (2010) Late Paleoproterozoic to early Mesoproterozoic Dongchuan Group in Yunnan, SW China: implications for tectonic evolution of the Yangtze Block. Precamb Res 182:57–69

Zheng JP, Griffin WL, O'Reilly SY, Zhang M, Pearson N, Pan Y (2006) Widespread Archean basement beneath the Yangtze Craton. Geology 34:417–420

Zhong H, Qi L, Hu RZ, Zhou MF, Gou TZ, Zhu WG, Liu BG, Chu ZY (2011) Rhenium-osmium isotope and platinum-group elements in the Xinjie layered intrusion, SW China: Implications for source mantle composition, mantle evolution, PGE fractionation and mineralization. Geochim Cosmochim Acta 75:1621–1641

Zhou M-F, Robinson PT, Lesher CM, Keays RR, Zhang CJ, Malpas J (2005) Geochemistry, petrogenesis, and metallogenesis of the Panzhihua gabbroic layered intrusion and associated Fe–Ti–V-oxide deposits, Sichuan Province, SW China. J Petrol 46:2253–2280